UNIVERSITY OF OKLAHOMA

GRADUATE COLLEGE

A DATA-DRIVEN APPROACH FOR THE EVALUATION OF SEISMICITY RISKS ASSOCIATED WITH CO_2 INJECTION

A THESIS

SUBMITTED TO THE GRADUATE FACULTY

in partial fulfillment of the requirements for the

Degree of

MASTER OF SCIENCE

By

KAREN IFEOMA OCHIE

Norman, Oklahoma

2022

A DATA-DRIVEN APPROACH FOR THE EVALUATION OF SEISMICITY RISKS

ASSOCIATED WITH CO_2 INJECTION

A THESIS APPROVED FOR THE
MEWBOURNE SCHOOL OF PETROLEUM AND GEOLOGICAL ENGINEERING

BY THE COMMITTEE CONSISTING OF

Dr. Rouzbeh Moghanloo, Chair

Dr. Hamidreza Karami, Co-Chair

Dr. Jeffery Burghardt, Co-Chair

Dedicated to my mother, who encouraged me to pursue graduate school.

ACKNOWLEDGEMENT

I would like to thank my advisor, Dr. Rouzbeh Moghanloo, for his constant support and tutelage. I am also grateful to Dr Hamidreza Karami and Dr. Jeffery Burghardt, for their time and support invested in me completing this thesis. I am also grateful to my team members on the Carbon Utilization and Storage Partnership (CUSP), working with them was very insightful and value adding.

I would also like to thank all the professors I assisted in teaching, Dr Chandra Rai, Dr Runar Nygaard and Dr Reza Zulfiquar, I enjoyed working with you and you made my stay worthwhile. I am also grateful to the Mewbourne Department of Petroleum Engineering, Francey Freeman, Sonya Grant, Katie Shapiro and Dominique Pittenger for making my leadership roles stress-free. To all the student organizations I worked with, you made my graduate school journey fun, thank you.

Finally, I would like to thank my parents: Chief and Mrs. Augustine Ochie, and my siblings: Samuel, Marypeace and Miracle for their unconditional love and care during my graduate school journey. To my partner, Chinedu Nwosu, my friends, and members of the Nigerian OU community, my journey would not have been complete without your contributions, I am indeed grateful.

Table of Contents

LIST OF FIGURES

LIST OF TABLES

ABSTRACT

This work examined the application of Bayes' theorem in evaluating the risk of induced seismicity associated with CO_2 sequestration in the Arbuckle Group, which extends across the southern Mid-Continent of the US. Geological storage can effectively contribute to reducing emission of CO_2, otherwise released into the atmosphere, achieving the climate goals committed in the 2021 United Nations Climate Change Conference (COP26). However, concerns about risks associated with CO_2 injection along with economic challenges of infrastructure required to execute the Carbon Capture Utilization and Storage projects stand against full realization of remarkable potentials. The main goal is usually for CO_2 to be stored over geologic time; hence, geomechanical risks such as the seismicity in the field or potential CO_2 leakage through seals cannot be ignored and is considered as one of the requirements to determine success of the project.

This work elaborated on the risk of potential seismic events that can impact the longevity and success of projects. Accurate risk estimation is key for environmental, economic, and safety concerns and is also one of the requirements to get class VI permits from the US Environmental Protection Agency. The increase of fluid injection in the Arbuckle Group and how it has increased seismicity risks was first demonstrated, and then utilizing the Bayesian approach, a statistical model where a random probability distribution is used to represent uncertainties within the model, including both input/output parameters to evaluate the seismicity risks was used to estimate these risks. Using the Arbuckle Group as a case study, established physics-based models of the system and the details from past observed/monitored failures was utilized to evaluate future risk potential for the area. In this approach, the current probability for the state of

stress for the area under investigation was established, then the evolution in the state of stress was monitored. The stress state probability distribution was calculated to evaluate the probability of activating a critically oriented fault over a range of specified pore pressures.

The results suggest seismicity risk is directly a function of fluid injection and that the probability of inducing seismicity in the formation can be estimated. Based on the modelling results, at initial injection pressures there is a 24% risk of introducing seismicity in the Arbuckle Group when a critically oriented fault exists. Based on these results, sensitivity analysis was conducted to determine the features that can impact the risk level. Introducing the stress state constraints from the Arbuckle Group in Kansas State, the risk of seismicity reduced to 12%.

Considering the results from this work, operators can optimize the site screening and collect additional data to constrain inherent uncertainties in geomechanical risk evaluation and make informed decisions during operations. The result from this work shows that geological storage of CO_2 with attention to seismicity risks in the Arbuckle formation can be a feasible safe strategy towards achieving climate goals in selected areas and there is value of information in obtaining stress data in these areas.

CHAPTER 1: Introduction

1.1 Problem Statement

There are many ways to ensure the world's energy needs are met while attempting to attain the world's energy sustainability goals, such as geothermal energy, hydropower, wind energy, solar energy, and so on. As shown in the figure below, there has generally been an increasing trend in the world's energy demand and consumption. This increase has also translated to an increase in sustainable energy. Despite this drive to move from an energy mix predominantly dominated by fossil fuels to these sustainable alternatives, fossil fuels still account for the bulk of the energy mix.

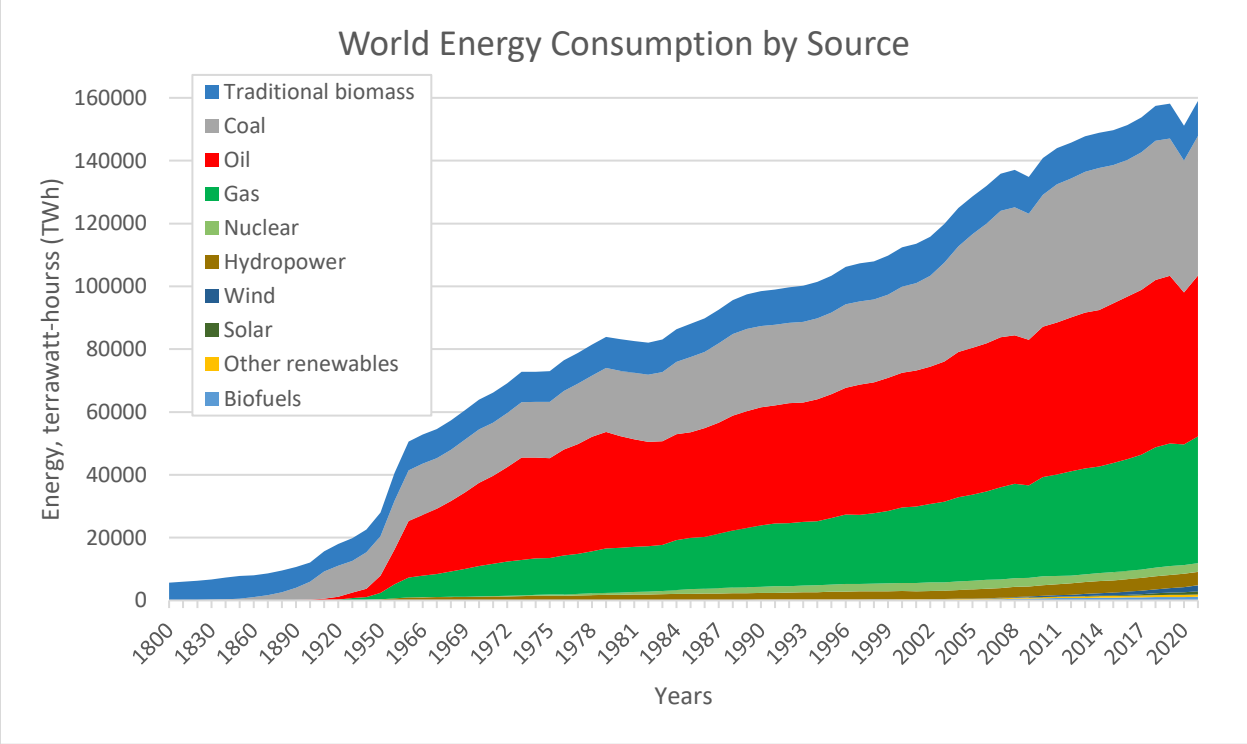

Figure 1: Energy Consumption in the World. Data source: (BP Statistical Review of World Energy , 2021)

Producing energy from fossil fuels is accompanied by carbon emissions into the atmosphere. Carbon emissions have been on a rapid increase in the past decade, as shown in the figure below, hence, there has been an interest in carbon sequestration, where the carbon released from fossil fuels is injected into the ground for storage over geologic time.

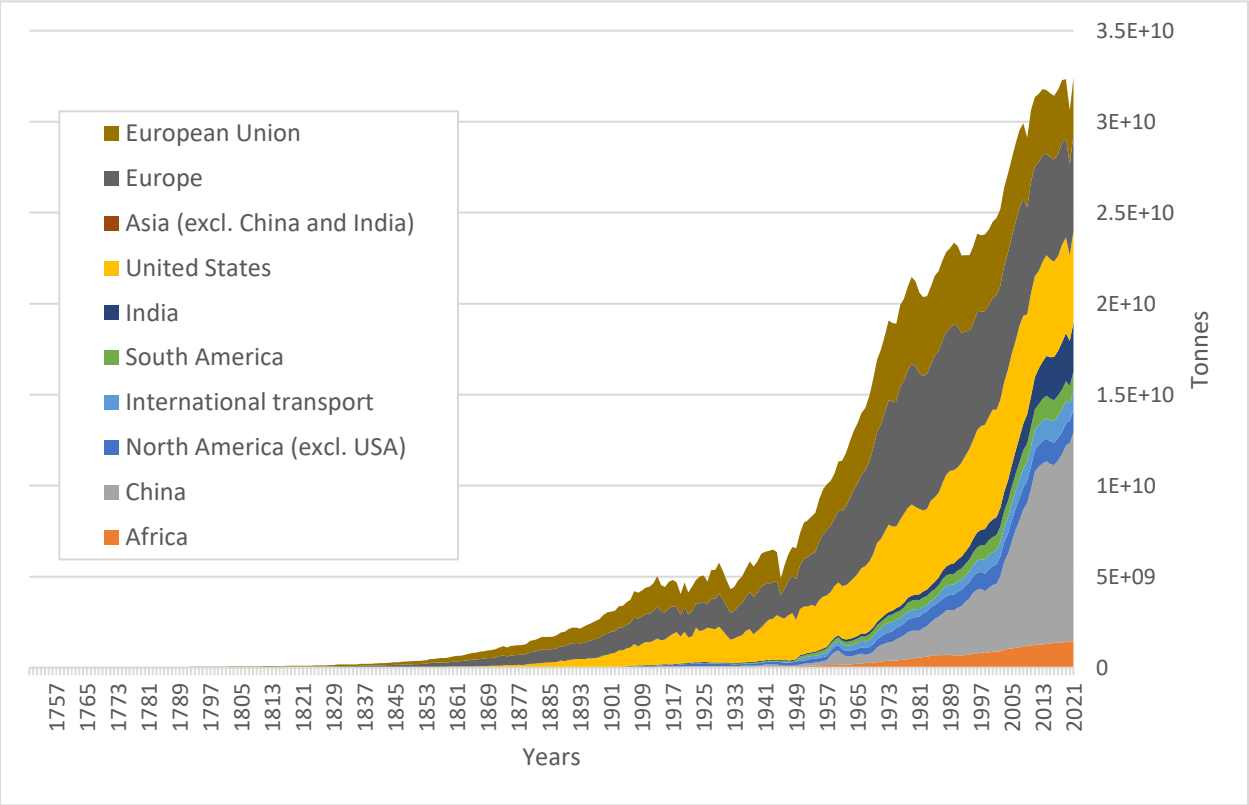

Figure 2: Annual Emissions of CO_2 from Fossil Fuels. Data source (Global Change Data Lab, 2022)

Geologic carbon sequestration works on the principle of capturing CO_2 from the atmosphere and storing it, so it is being prevented from being emitted back into the atmosphere. In the conventional oil and gas industry, this technology has been used to improve productivity, known as enhanced oil recovery (EOR) (Battelle, 2018). It has however currently gained more popularity as the capturing and storing of carbon dioxide (CO_2) can effectively decrease greenhouse gases emissions into the atmosphere – as CO_2 is one of the most common greenhouse

gases – while achieving the energy and climate goals committed at the 2021 United Nations Climate Change Conference (COP26). Asides from EOR, captured CO_2 can also be used in gas processing to clean natural gas and power plants also CO_2 capture to reduce carbon emissions.

Injection into the formation has been shown to cause induced seismicity risks in the formation for storage and surrounding formations. Different applications in the traditional hydrocarbon industry have historically been interested in determining the extent of seismicity risks in geologic formations particularly as hydrocarbon investigation ventured into deeper terrains with more challenges (Burghardt, Geomechanical Risk Assessment for, 2018). Since the 1990s when geomechanical risks in geologic carbon storage (GCS) picked up interest, research showed that there is substantial geomechanical changes with change in injection pressures (Rutqvist, 2012), (Bissell, et al., 2011), (Verdon, Kendall, White, & Angus, 2011), (Zhou, Birkholzer, Mehnert, Lin, & Zhang, 2010). According to (Ajayi, Gomes, & Bera, 2019), storing CO_2 in geologic formations entails that the formation must be suitable for storage and the injected plume has to be monitored consistently over time to ensure that there is proper containment.

In geologic carbon sequestration, where geomechanical risks have as much significance as resource-related risks, with risks historically increasing in importance with time and being of long-term impact, there is need to have more certainty in the risk assessments, especially as the main goal in carbon sequestration is typically for CO_2 to be stored over geologic time. Geomechanical risks such as the seismicity in the field or potential CO_2 leakage through seals can therefore not be ignored and are considered as part of the requirements for project feasibility determination.

Quantifying the risks for geologic carbon sequestration – such as the risk of seismicity with a high degree of certainty is not just necessary for accuracy but is also a key safety, environmental, and economic concern. It is also one of the requirements to get class VI permits from the US (United States) Environmental Protection Agency (EPA, Geologic Sequenstration of Carbon Dioxide. Underground Injection Control (UIC) Program Class VI Implementaion Manual for UIC Program Directors, 2018). Significant seismic activities and how they affect the feasibility of CO_2 storage, as well as the reception of CO_2 sequestration by the general public has recently been of concern. In the past, projects in the Netherlands and Germany have been required to be postponed on account of concerns regarding risks to the public such as possible seismic tremors, spillage and leakage, and effect on property (Rutqvist, 2012). Subsequently, large-scale GCS must be created with consideration, and geomechanics is a key part of risk examinations in geologic carbon sequestration sites. In this research, the increase of seismicity risks in the Arbuckle Group is demonstrated and then a Bayesian approach is used to evaluate these seismicity risks.

Risk is a combination of the probability of an adverse event occurring and the severity of that event. Since the level of risk could come from events of different severity, it is important to quantify the uncertainties in risk evaluation. The Bayesian approach is a statistical model where the uncertainty (both output and input/parameters) in the model is represented as a probability distribution, and this can be used to quantify the seismicity risks and improve risk assessment. Using the Arbuckle Group as the area of study, data from established physics-based models of the system and the details from past observed/monitored failures as shown in figure 3, was utilized to evaluate future risk potential for the area. In this approach, the current probability for

the state of stress for the area under investigation was established, then the evolution of the state of stress owing to subsurface fluid injection. The state of stress probability distribution is then calculated to estimate the probability of activating a critically oriented fault.

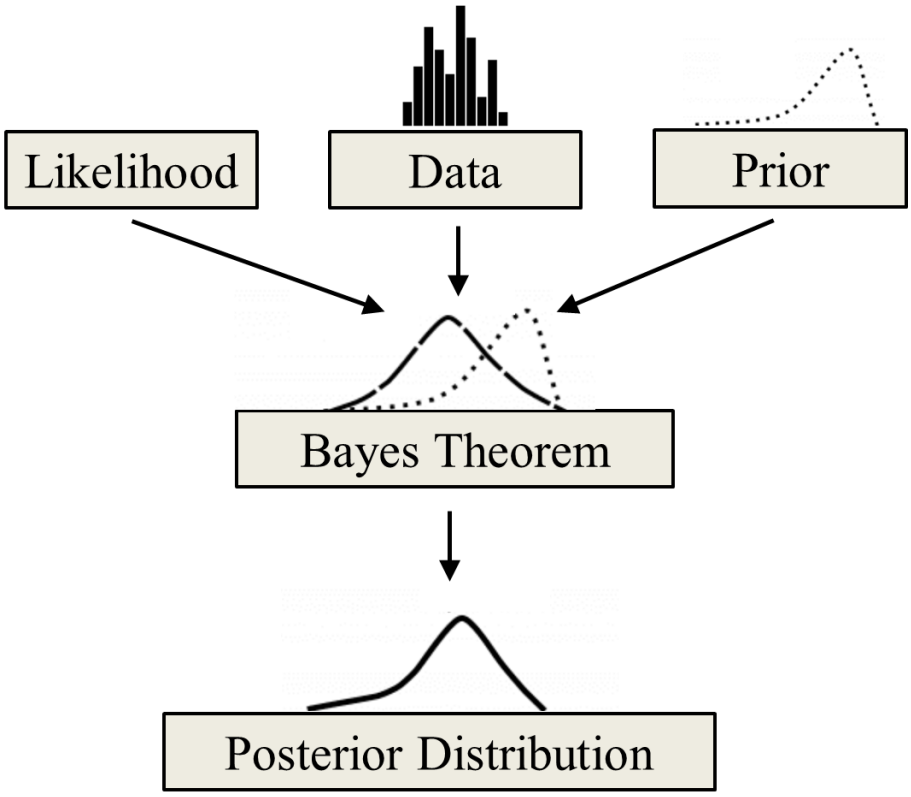

Figure 3: Bayesian Approach in Essence. Adapted from (Nelidov, 2021)

1.2 Objectives

This study has the following main objectives:

- Demonstrate the need to estimate seismicity risk in CO_2 sequestration using a data-driven approach
- Quantitatively estimate induced seismicity risk when injecting into the Arbuckle Group

1.3 Scope of the Thesis

The scope of this thesis is to demonstrate how fluid injection has increased seismicity risks in the Arbuckle Group which extends across the southern Mid-Continent of the US, and how these risks of induced seismicity associated with CO_2 sequestration can be quantified.

1.4 Working Hypothesis

The working hypothesis is that using Bayes' theorem can assist in evaluating the risk of induced seismicity.

1.5 Organization of the Thesis

This thesis is sub-divided into five chapters:

- Chapter 1: Introduction to the concept, including the objective of the thesis, scope of the thesis, and organization of the thesis
- Chapter 2: Literature review on carbon sequestration and the importance of determining seismicity risks
- Chapter 3: Explains the proposed methodology for determining seismicity risks
- Chapter 4: Explains the results obtained from the modeling and its interpretation
- Chapter 5: The conclusion of the study

CHAPTER 2: Literature Review

2.1 Geologic Carbon Sequestration

Geologic Carbon Sequestration (GSC) is storing captured carbon in a geologic formation over geologic time – over thousands of years (International Energy Agency, 2016). The technology had initially been implemented since the 1920's in the separation of CO_2 from saleable methane gas in natural gas reservoirs (IEAGHG, 2022). This concept gained more popularity in the 1970's when captured CO_2 was injected in an oil field in Texas to boost productivity from the formation and was called enhanced oil recovery (EOR) in the conventional oil and gas industry (Battelle, 2018). However, it has currently gained more popularity as it can effectively decrease greenhouse gases emissions. The types of geologic formation for CO_2 sequestration are broadly classified into depleted oil and gas reservoirs, saline aquifers, unmineable coal beds and shales shown in figure 4 below. The kind of seismicity risks encountered in the geologic formation are highly dependent on the type of formation.

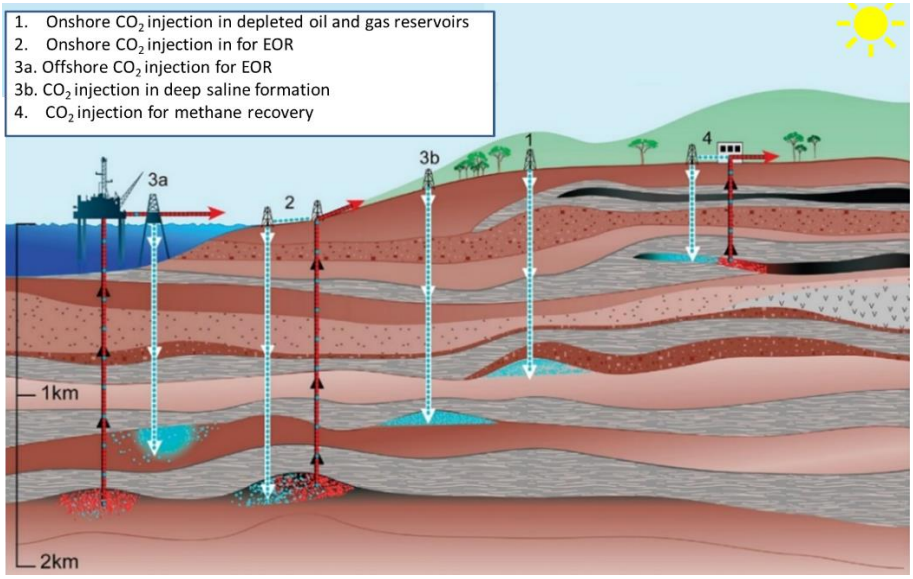

Figure 4: Overview of Geologic Carbon Sequestration. Modified from (Intergovernmental Panel on Climate Change, 2005)

2.1.1 Storage in Aquifers

Saline aquifers have been identified as one of the most promising geologic storage sites for the storage of CO_2. The main goal in any CO_2 sequestration project is typically for the CO_2 to be stored for a long period of time. Hence, monitoring the CO_2 plume when storing the CO_2 in aquifers is particularly important because the injected CO_2 has a propensity for migrating upwards since it is less dense than the water in the aquifer (Barrufet, Bacquet, & Falcone, 2010). Brine migration and stress changes due to pressure increase from sequestration are key challenges when storing CO_2 in aquifers. Stress changes can result in fault reactivation, increased seismicity, formation or caprock fracturing, or surface uplifting (Bandilla, Celia, Birkholzer, Cihan, & Leister, 2015). This means that geomechanical risks such as seismicity in the field or potential CO_2 leakage through seals must be considered.

2.1.2 Storage in Hydrocarbon Reservoirs

Over the years, hydrocarbon reservoirs have shown exciting potential as geologic sites for CO_2 storage, especially as they have stored hydrocarbons for prolonged periods of geologic time. This is important because their past exploration, exploitation, and production, knowledge of their architecture and properties can be leveraged for CO_2 storage projects (Chidambaram, Tewari, Ali, Tan, & PETRONAS, 2021). Since producing hydrocarbons contributes to increasing CO_2 emissions, planning for sequestration is beneficial for climate goals. Storage in hydrocarbon reservoirs can be of two forms. It can be stored via EOR, which is more popular as it generates revenue upon implementation and has been practiced before CO_2 sequestration even became a solution for excessive CO_2 emission. The second form is storage in depleted reservoirs which is a relatively more recent technology.

2.1.3 Storage in Coal Bed

CO_2 sequestration in unmineable coal seams is of interest because of the concurrent recovery of methane while storing the CO_2 (Gorucu, et al., 2005). This results in decreasing atmospheric CO_2 concentrations while reducing the associated costs of handling CO_2 during methane production. Producing methane is also a source of CO_2 emissions, hence planning for sequestration is also beneficial to the environment. To study CO_2 storage capacity in coalbed reservoirs, adsorption and desorption experiments of coal rocks from different regions and coal ranks need to be conducted (Jiang, Dou, Shen, & Sun, 2015)**.**

2.1.4 Storage in Shales

Storing CO_2 in shales is not as popular despite them being abundant, as they typically have extremely low permeability, and the field implementation is not as developed as other geologic storage sites. (Fakher, Abdelaal, Elgahawy, & El-Tonbary, 2020) and (Fakher & Imqam, 2020) demonstrated the advantage of using shales to store CO_2 by considering the main mechanism for storage to be absorption, and they showed the absorption capacities of different shale plays at different thermodynamic conditions.

Each of the geologic sites has different trapping mechanisms. A trapping mechanism and the geologic site properties would determine the type of deformation that might be encountered and overall, the efficiency of the sequestration. Trapping mechanisms can be generally classified as physical or geochemical, as shown in the figure below. Physical trapping mechanisms can either be when structural or stratigraphic traps entrap mobile CO_2 or when CO_2 becomes trapped in pore spaces due to its lack of mobility at irreducible saturations (Bachu, 2008), (Benson & Cole,

2008). Geochemical trapping involves the dissolution of CO_2 in in-situ fluids. This can be because of the solubility of the fluids or ions in the fluids entrapping the CO_2. Aside from reaction with in-situ fluids, geochemical tapping can also occur when the CO_2 reacts with the matrix of the formation. This is called mineral trapping. During CO_2 injection, geomechanics is most related to physical trapping, hence the seismicity risk is associated with physical trapping.

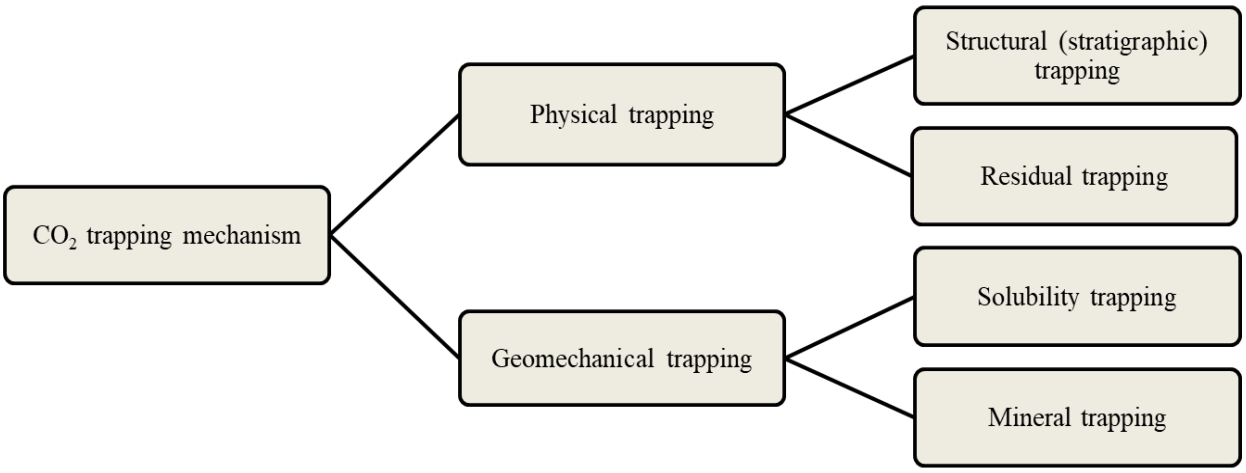

Figure 5: Different CO2 trapping mechanisms in geological storage sites

2.2 Geomechanical Risk

Risk is the probability of occurrence and magnitude of consequence of an unwanted accident. It is a combination of the probability of an adverse event occurring and the severity of that event. Under this concept a given level of risk could come from events of different severity, but the more severe the event the lower the probability of its occurrence would be. In geologic subsurface sequestration activities, achieving zero geomechanical risk is nearly impossible, majorly due to the limited direct access to the deep subsurface via boreholes and the inherent heterogeneity of geology, hence it is incredibly significant to be able to estimate the probabilities

of the state of stress associated with these activities as well as other geomechanical parameters that can contribute to the risk of sequestration.

The Environmental Protection Agency (EPA) has some well-laid out guidelines regarding the risks associated with CO_2 injection. The Class VI permit regulations (EPA, Subpart UU – Injection of Carbon Dioxide, 2021) require that an operator should submit relevant information on stress, and in situ fluid pressures, fractures, rock strength and ductility. They should also demonstrate that the proposed injection pressures and volumes into the formation would not initiate or propagate faults or fractures (EPA, Subpart UU – Injection of Carbon Dioxide, 2021). The fracture pressure should exceed the injection pressure, that is, the injection pressure should not be more than 90% of formation fracture pressure, such as in (Chiaramonte, Zoback, Friedmann, & Stamp, 2008) and (Zoback, et al., 2003). Hence, direct in situ formation testing, hydraulic fracture tests, borehole breakouts, and drilling induced fractures tests (DIFT) should be applied to evaluate the complete stress tensor hence, determining the magnitudes of the principal minimum horizontal stress and principal maximum horizontal stress with considerable accuracy.

(Ringrose, et al., 2013) explained the geomechanical risks associated with geologic carbon sequestration as shown in figure 6 below. They highlight that changes in the formation can occur beyond the point of injection and even the CO_2 plume. It can be observed that changes in the temperature and pressure in the area of injection can cause changes in the stress and mechanical strain patterns, and fault activation around the area of injection. Beyond this area, stress and strain changes can also occur and these can affect faults, resulting in seismic events.

Based on these highlighted geomechanical risks, it is apparent that accounting for these risks has a significant part to play when selecting a site for carbon sequestration. At the early stages of

carbon sequestration projects, risk assessments is usually performed to determine if the site is fit for selection (Stauffer, Viswanathan, Pawar, & Guthrie, 2009); (Oldenburg, Bryant, & Nicot, 2009). In such an analysis, the risks involved is not just limited to seismicity risks but also captures other events such as CO_2 leakage into the formation, CO_2 migration and buoyancy effects, contamination of groundwater table and aquifers due to carbon sequestration, deformation of surrounding formation and overlying seals, localized deformation around the point of injection, well damage due to injection CO_2, migration to surface via faults or leaky pathways, and so on.

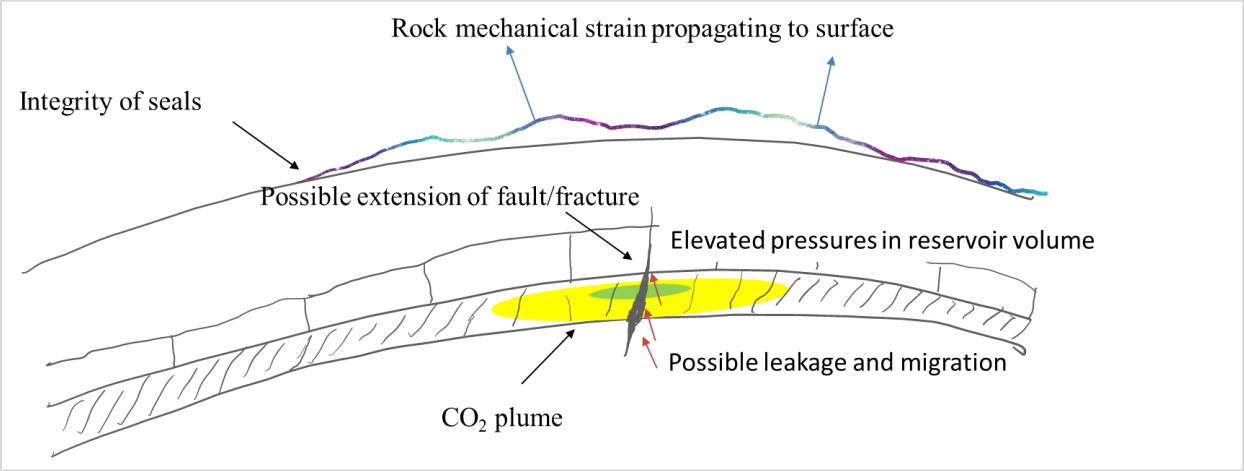

Figure 6: Geomechanical risks associated with GCS in deep sedimentary rock rocks. Modified from (Ringrose, et al., 2013)

2.3 Methods for Determining Geomechanical Risk

There are several methods available to obtain the magnitudes and directions of geomechanical parameters, however when utilizing these parameters to quantify or estimate the geomechanical risk, the scope becomes narrower. Several research projects have been conducted to calculate the geomechanical risk implications of a project, and they are broadly divided into simulation methods and analytical methods.

In the empirical method, it entails obtaining a document known as a risk register, estimating the risks involved in executing the project, and then determining the expected impact of the risk. The challenge with this technique is that it requires the knowledge of the subject matter experts, and the success of the project is heavily dependent on their capacity. The value obtained from this technique is dependent on the sequestration project hence there is still need to capture uncertainties before the project commences (White, Foxall, C. Bachmann, & Daley, 2015).

In the simulation method, hydro-mechanical models are applied to simulate the required pressure to induce seismicity risks (White, Foxall, C. Bachmann, & Daley, 2015). It is however important to account for the uncertainties in the model. A popular technique known as Monte Carlo simulation can be used to determine these uncertainties. The Monte Carlo simulation obtains the likelihood of a range of results using a repeated random sampling. While this simulation is easy to implement, it also requires that the samples are uncorrelated, random, and independent on each other (Burghardt & Appriou, State of Stress Uncertainty Quantification and Geomechanical Risk Analysis for Subsurface Engineering, 2021). The limitation with this approach is that if the stress state is being constrained by frictional faults, known as the stress polygon approach, it is defined by the principal stresses' ratio (Burghardt & Appriou, State of Stress Uncertainty Quantification and Geomechanical Risk Analysis for Subsurface Engineering, 2021). This means that the geomechanical properties such as the principal minimum horizontal stress and the principal maximum horizontal stress are related to each other, hence the inherent assumption that the samples in the Monte Carlo simulation need to be unrelated and random no longer holds.

(Burghardt & Appriou, State of Stress Uncertainty Quantification and Geomechanical Risk Analysis for Subsurface Engineering, 2021) presented a solution to this limitation by using the

Bayesian approach. Here, they were able to represent the samples as a stress polygon approach utilizing a joint probability of the principal minimum horizontal stress and the principal maximum horizontal stress. They officially implemented this approach in a tool known as the State of Stress Analysis Tool (SOSAT). It was implemented as part of the National Risk Assessment Partnership (NRAP), a funded project the US (United States) Department of Energy's Office of Fossil Energy.

Table 1: Estimation of Seismicity Risks

Method	**Approach**	**Limitation**
Empirical Analysis	It entails estimating the risks involved in executing the project, and then determining the expected impact of the risk by SMEs.	The value obtained relies on values after and during injection. (White, Foxall, C. Bachmann, & Daley, 2015) Capturing uncertainties before the project commences still required.
Monte Carlo Simulation	Obtains the likelihood of a range of results using a repeated random sampling. While this simulation is easy to implement, it also requires that the samples are uncorrelated, random, and independent on each other.	If stress state is constrained by frictional faults, it is defined by the principal stresses' ratio (Burghardt & Appriou, 2021), hence, geomechanical properties such as σh and σH are related to each other. The inherent assumption that the samples need to be unrelated and random no longer holds.

State of Stress Analysis	(Burghardt & Appriou, State of Stress Uncertainty Quantification and Geomechanical Risk Analysis for Subsurface Engineering, 2021) presented a solution to this limitation by using the Bayesian approach.	Generates the stress state for a single point.

CHAPTER 3: Methodology

3.1 State of Stress Analysis

It has been established that the injecting CO_2 in geologic formations is accompanied by an increase in pore pressure which would contribute to a change in the state of stress. This could potentially influence the geomechanical risks due to induced seismicity and migration of fluid. To mitigate these risks, understanding the behavior of in-situ stresses over geologic time is very important.

In the formation, three orthogonal principal stresses which are perpendicular to each other are used to define the stresses in the formation. The vertical stress is a function of the mass density of the overburden of the formation and its true vertical depth. It can be a principal stress, but this is not always the case. Once the vertical stress has been established as a principal stress, the remaining stresses are the minimum horizontal stress and the maximum horizontal stress.

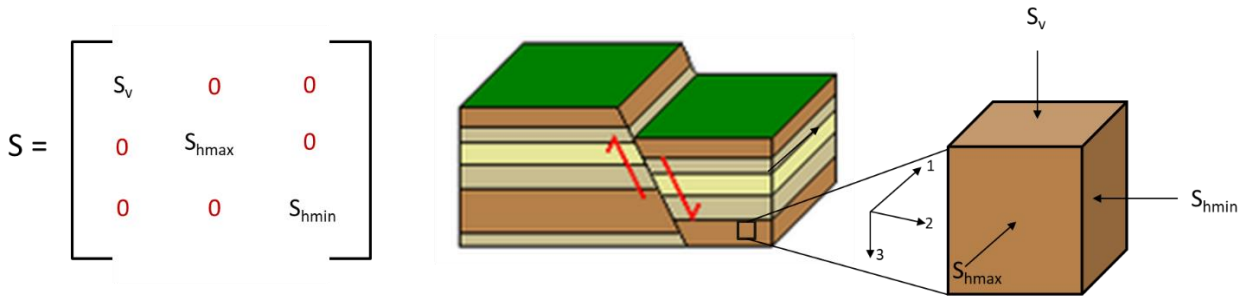

Figure 7: Principal Stresses. Modified from (Espinoza, 2020)

Depending on the relative magnitudes of each principal stress, there are three different types of fault regimes which can result:

1. Normal faulting (NF) is when the largest principal stress is the vertical stress, and the minimum principal stress is horizontal. Normal faulting regimes are common in passive or extensional environments (Espinoza, 2020).
2. Strike-slip faulting (SS) faulting is a regime where both the maximum and minimum principal stresses are in the horizontal plane, which is common in regions with tectonic shearing (Espinoza, 2020). The max horizontal stress is greater than the vertical stress which is greater than the minimum horizontal stress.
3. Thrust faulting (TF) is the scenario where the maximum principal stress is in the horizontal direction and the minimum principal stress is the vertical stress. This is common in tectonically compressive regions (Espinoza, 2020).

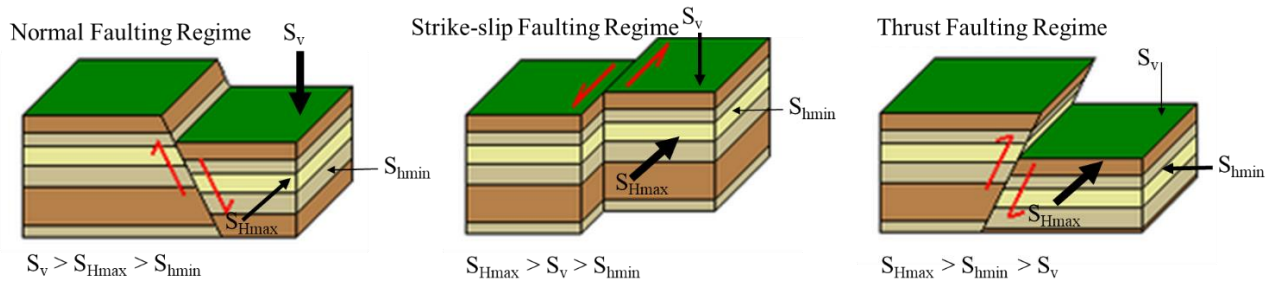

Figure 8: Different Stress Regimes. Modified from (Jaffar & Abdulnaby, 2018)

Recall that if the stress state is being constrained by frictional faults, it is defined by the principal stresses' ratio hence the minimum horizontal stress and maximum horizontal stress are related and cannot be modelled as statistically independent. To account for this, the stress polygon approach is used to capture this relationship. This approach has an assumption that the state of

stress for any pore pressure or true vertical depth has a frictional strength limitation due to the faults with critical orientation to stress field and already existing fractures.

3.2 Model Formulation

Despite the necessity of understanding the behavior of in-situ stresses over geologic time to mitigate these seismicity risks, it is however, not always feasible as site specific stress measurements are not readily available and there is significant uncertainty in the stress state. Incorporating the stress polygon approach and of Thiercelin and Plumb's 1D tectonic-elastic approach, (Burghardt, SOSAT, 2021) developed a method for estimating the state of stress for a given location subsurface called the State of Stress Analysis Tool (SOSAT).

According to (Burghardt & Appriou, State of Stress Uncertainty Quantification and Geomechanical Risk Analysis for Subsurface Engineering, 2021) described that for slip to occur in a fault, it is defined by the relation:

$$\frac{S_1 - P_p}{S_3 - P_p} = [(\mu^2 + 1)^{\frac{1}{2}} + \mu]^2 \quad (1)$$

Where:

S_1 = greatest principal stress

$Pp =$ is the pore pressure

S_2 = least principal stress

μ = coefficient of friction

For the different stress regimes, this equation assumes the Anderson's theory of faulting in the limitation on the ratio of stress differences as illustrated in the figure below (Appriou, 2019).

According to (Zoback, et al., 2003), the stress polygon approach assumes that given a specified pore pressure and coefficient of friction, the stress at which shear failure occurs must be greater than the difference in stress magnitudes (Appriou, 2019).

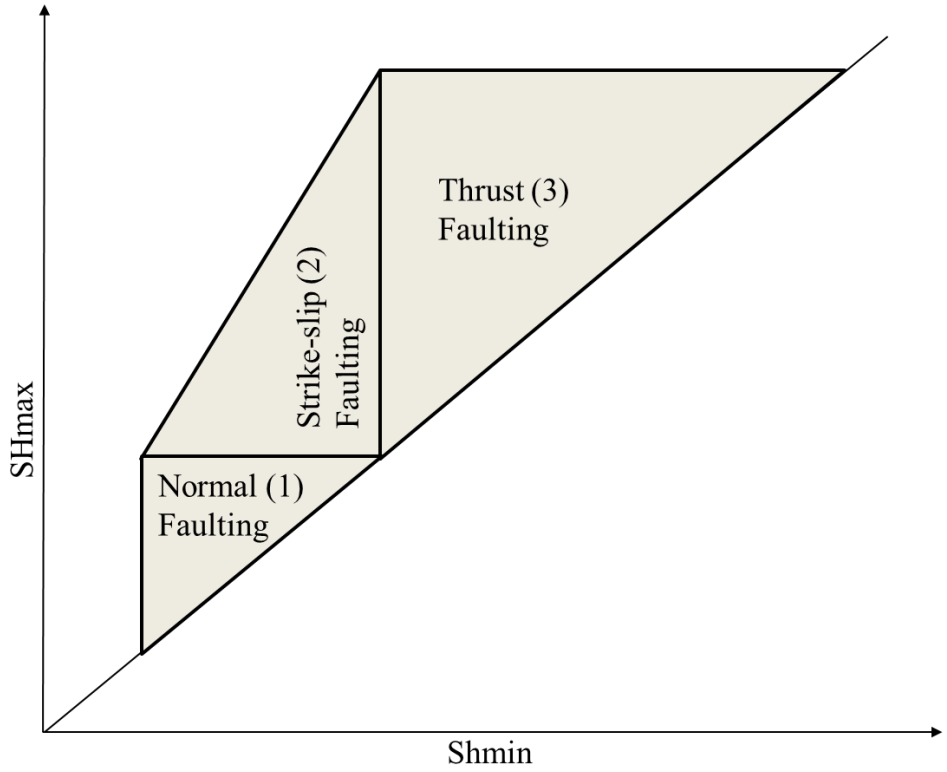

Figure 9: Stress polygon approach for in situ stress determination in SOSAT. Modified from (Appriou, 2019)

1. If Sv is the greatest stress and Sh is the least stress, *Sv* > *Shmax* > *Shmin*, then the differential stress magnitude is affected by the normal faulting regime.

   Equation 1 becomes modified to,

$$\frac{\sigma_1}{\sigma_3} = \frac{S_v - P_p}{S_{hmin} - P_p} \leq [(\mu^2 + 1)^{\frac{1}{2}} + \mu]^2 \qquad (2)$$

2. If Shmax is the greatest stress and Shmin is the least stress, *Shmax* > *Sv* > *Shmin*, then the differential stress magnitude is affected by the strike-slip faulting regime.

   Equation 1 becomes modified to,

$$\frac{\sigma_1}{\sigma_3} = \frac{S_{hmax} - P_p}{S_{hmin} - P_p} \leq [(\mu^2 + 1)^{\frac{1}{2}} + \mu]^2 \quad (3)$$

3. If Sv is the least stress, *Shmax* > *Shmin* > *Sv*, then then the differential stress magnitude is affected by the thrust faulting regime.

   Equation 1 becomes modified to,

$$\frac{\sigma_1}{\sigma_3} = \frac{S_{hmax} - P_p}{S_v - P_p} \leq [(\mu^2 + 1)^{\frac{1}{2}} + \mu]^2 \quad (4)$$

The next portion of the model development is the 1D tectonic-elastic model proposed by Thiercelin and Plumb in 1994 (Appriou, 2019). The approach assumes the of the three principal stresses, one is vertical, occurring at a particular true vertical depth and with a specific overburden weight, represented by the equation below,

$$S_v = \int_0^z \rho(z) g dz \quad (5)$$

The horizontal principal stresses can then be calculated using the linear poroelasticity equations for horizontal stresses as shown below,

$$S_{hmin} = \frac{E_h}{E_v} \frac{v_{hh}}{1 - v_{vh}} (S_v - \alpha_v P_p) + \frac{E_h}{1 - {v_{hh}}^2} (\varepsilon_H + v_{hh} \varepsilon_H) + \alpha_h P_p \quad (6)$$

$$S_{hmax} = \frac{E_h}{E_v} \frac{v_{hh}}{1 - v_{vh}} (S_v - \alpha_v P_p) + \frac{E_h}{1 - {v_{hh}}^2} (\varepsilon_H + v_{hh} \varepsilon_H) + \alpha_h P_p \quad (7)$$

Where:

E_h = horizontal Young's modulus

E_v = vertical Young's modulus

v_{hh} = horizontal-horizontal Poisson's ratio

v_{vh} = vertical-horizontal Poisson's ratio

α_h = horizontal component of the Biot coefficient tensor

α_v = vertical component of the Biot coefficient tensor

ε_H = maximum horizontal strain

ε_h = minimum horizontal strain.

Based on these highlighted equations, the stress state is dependent on the overburden weight, the poroelastic properties, and the horizontal strain (Appriou, 2019). Incorporating this with the stress polygon and Bayesian approach to account for uncertainty, SOSAT was developed. It is a publicly available, open-source tool created as part of the NRAP project to assist with performing geomechanical risk analysis using the Bayesian model and commonly available data. The tool presented the stress polygon approach utilizing a joint probability of the principal minimum horizontal stress and the principal maximum horizontal stress. The tool allows the user to specify the probability distributions for relevant parameters (Burghardt & Appriou, State of Stress Uncertainty Quantification and Geomechanical Risk Analysis for Subsurface Engineering, 2021) in assessing seismicity risks.

During site screening for Geologic Carbon Sequestration projects, the tool can add value by identifying the additional data required that would better define or constrain the uncertainties in the geomechanical risk quantification, enabling operators to make appraised operational

decisions, build stakeholder engagement and confidence, and understand and manage geomechanical risks better (Burghardt & Appriou, State of Stress Uncertainty Quantification and Geomechanical Risk Analysis for Subsurface Engineering, 2021).

To address the challenge of the analytical method, a Bayesian method is used to account for the uncertainty in the input parameters and to generate the probability of activating a critically oriented fault over a range of input parameters.

3.3 Bayesian Model

The Bayesian approach is a statistical model which uses a random probability distribution to represent the uncertainties in the model. This includes both input/output parameters and is used for risk evaluation in this work. It is based on the Bayes' theorem which is a data analysis approach where the information in observed data is used to update the available knowledge about parameters in a statistical model. In the Bayesian workflow, there are three main steps shown in figure 10. The first is obtaining accessible prior knowledge of the statistical model parameter. This is done through the prior distribution and can be from physical models, expert belief, or previous empirical data. The next is then determining the probability function using the newly observed data. The last step involves merging these two steps to create a posterior distribution, which shows the updated knowledge, which balances the prior knowledge with new data, and can then be used for inferences and making predictions.

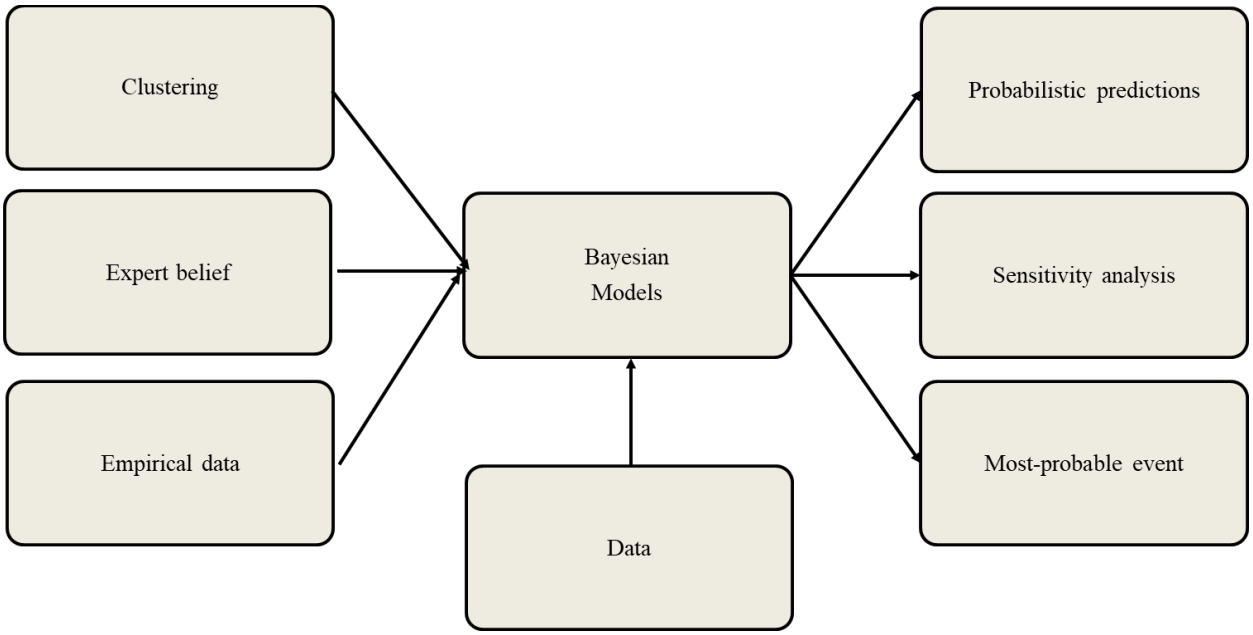

Figure 10:An example of inputs and outputs of a Bayesian network

3.3.1 Applications of Bayesian Model

Bayesian inference performs well with sparse data, and the results of the model can be easily interpreted and is easily understandable. This makes it a preferred method because it is simple to use the current knowledge of the world with a relatively small or unclean data set to predict the outlook of the world. Based on this, there have been several applications of the Bayesian Model.

In business and commerce, Bayesian Models are commonly used for pricing decisions and in new product development (Open Data Science, 2021). It can be used to determine prices of goods based on the market size and share, and wholesale and retail prices – field data. It can also be used to evaluate the risk of a project based on the uncertainties involved (Coyle, 2018). It can also be used for product ranking and customized user experience in online shopping.

In the marketing sector, organizations use past marketing campaigns and data to improve existing ones and create new ones. They also use it for targeted marketing like customized emails

and website and graphic designs based on user engagement (Open Data Science, 2021). The stock markets also use Bayesian networks to forecast future stock trends based on current and previous trends.

In the field of science, Bayesian deep learning can be used for weather forecasting, however, this is still recent research. Researchers have also used it to identify the underlying risk of diseases. They use it to consider group and individual risk factors, and variables that enhance disease spread (Open Data Science, 2021). Doctors also use this approach in diagnosing patients by looking at their medical history, family history, lifestyle and so on.

In summary, Bayesian models are best applied where there is noisy and heterogeneous data. It can be applied where better understanding of the uncertainties is required (Coyle, 2018).

3.3.2 Bayesian Model in Stress Determination

In-situ stress uncertainty can be classified as either parametric uncertainty or model form uncertainty. Parametric uncertainty is due to the uncertainty in the model parameters while model form is due to the approach of modeling for describing the physics of the system that causes stress. Both are important and make up the total uncertainty, which is a risk analysis input. To minimize model form uncertainty, the parametric uncertainty should however be quantified. This is because determining which model best fits the data is the only way to address the model form uncertainty. The shortcoming with this technique is that choosing a model that fits the data best would benefit models with the highest parameter count, regardless of the physics behind the data. Also, the statistical difference between the different models is not considered. Using a Bayesian model addresses these limitations as each model selection and

associated assumptions are considered as competing hypotheses for testing. Since model selections with unbound parameters will have larger uncertainties, this technique clearly benefits simpler model selections unlike the deterministic approach, which benefits more complicated models.

Oftentimes, there is a correlation between the two horizontal principal stresses. This means that treating them as independent properties is not representative, hence, they should statistically be considered a joint probability distribution (of magnitude and direction), shown in the figure below. The Bayesian relationship is represented in equation 1 below:

$$P(\sigma_H, \sigma_h|D) = \frac{P(D|\sigma_H, \sigma_h)P(\sigma_H,\sigma_h)}{P(D)} \quad (1)$$

Where:

$P(\sigma_H, \sigma_h|D) =$ **Posterior distribution:** the probability of (σ_H,σ_h) after the observation

$P(D|\sigma_H, \sigma_h) =$ **Likelihood:** how likely would the observation be for a given value of (σ_H,σ_h)

$P(\sigma_H, \sigma_h) =$ **Prior distribution:** probability of a given value (σ_H,σ_h) given everything else we knew before the observation

Applying the Bayesian model, the posterior joint probability distribution of the current stress state is first computed. Using random samples from this posterior distribution, the probability for a critically oriented fault to be activated is then computed in a neighborhood of different pore pressures, to evaluate how the stress is expected to change with pore pressure. The next step is to

quantify the certainty of current stress state by evaluating the probability for a critically oriented fault to be activated is then estimated for a neighborhood of different pore pressures using the pre-determined state of stress probability distributions as an input.

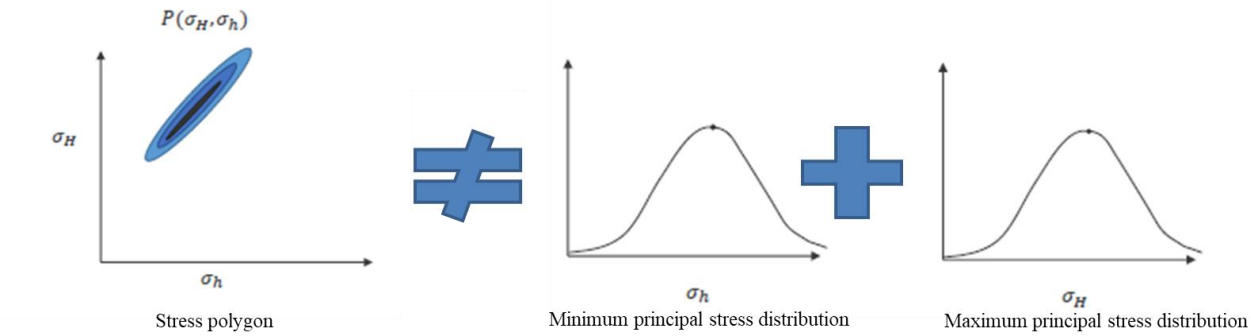

Figure 11: Stress as Joint Probabilities. Modified from (Burghardt, SOSAT, 2021)

3.4 Data Requirements

The main parameters required are the reservoir properties, the regional stress information, and the stress measurement parameters.

3.4.1 Reservoir properties

Reservoir Depth: this parameter is the true vertical depth (TVD) of this location.

Pore pressure gradient: the expected pore pressure at this depth, divided by the TVD.

Average overburden density: it is the average density of the formations overlying the depth of interest. Ideally this would be calculated using density logs all the way to the surface. In cases where density logs are available, but do not extend to the surface, there are methods for extrapolating it in a reasonable way. In cases where density logs are not available, then a

reasonable average value can be used with knowledge of the lithology of the overlying formations, or from nearby wells where density logs are available.

Maximum injection pressure: this is the maximum pore pressure that will be used in the fault activation probability calculations. This parameter is expressed in terms of the total gauge pressure, not as an overpressure relative to the initial formation pressure.

Median friction coefficient and Standard Deviation of logarithm of fault friction coefficient: frictional properties of specific faults and fractures existing at a given site is generally not feasible to collect, hence significant uncertainty remains in which frictional properties should be used. SOSAT uses a lognormal distribution for the friction coefficient. Fictional properties have been measured in the laboratory, and inferred from field data, for a wide variety of rock and interface types. These data show that a typical value of the friction coefficient is 0.6–0.7, but occasionally values much lower or greater than this have been measured. The default values in the SOSAT are 0.7 for the median of the friction coefficient, and 0.15 for the standard deviation of the logarithm of the friction coefficient.

Maximum possible friction coefficient: according to the (Burghardt, Geomechanical Risk Assessment for, 2018)'s knowledge friction coefficients in excess of about 1.5 have not been observed with any rock types.

3.4.2 Regional Stress Info Parameters

Normal faulting weight, Strike-slip faulting weight and Thrust faulting weight: The three weights are relative in the sense that their absolute magnitude does not matter, only their relative magnitudes.

K-thrust and K-SS: these are logistic function parameters that control the shape of the transition between the different faulting regimes. A larger value means the regime would transition abruptly.

3.4.3 Stress Measurement Parameters

Mean of the minimum principal stress measurement and Standard deviation of the minimum principal stress measurement: Stress measurements based on mini-frac or extended leak-off (XLOT) tests typically use a set of assumptions about the induced fracture geometry and behavior. Most commonly, it is assumed that the fracture is planar and opens under pure tensile opening and that leaks off into the formation follows a relatively simple functional relationship that is independent of pressure. A normal distribution is used to represent the mean and standard deviation.

3.5 Introduction to Area of Study

The Arbuckle Group underlays most of Oklahoma, Kansas, and adjacent states and was deposited during the Middle Cambrian to Late Ordovician period (Ching & Friedman, 2000). The lithology is mostly sandstone, limestone, and dolomite with dolomitic shale (Rottmann, 2018). The Oklahoma Geological Survey provided access to cores from the group and when one core with its in-situ location located near many of the disposal wells was studied by (Daneshfar, Hughes, & Civan, 2009) at the University of Oklahoma to analyze its composition. About 90% of the core was dolomite with the remaining indicating calcite, illite, quartz, and pyrite as listed in Table 1 below.

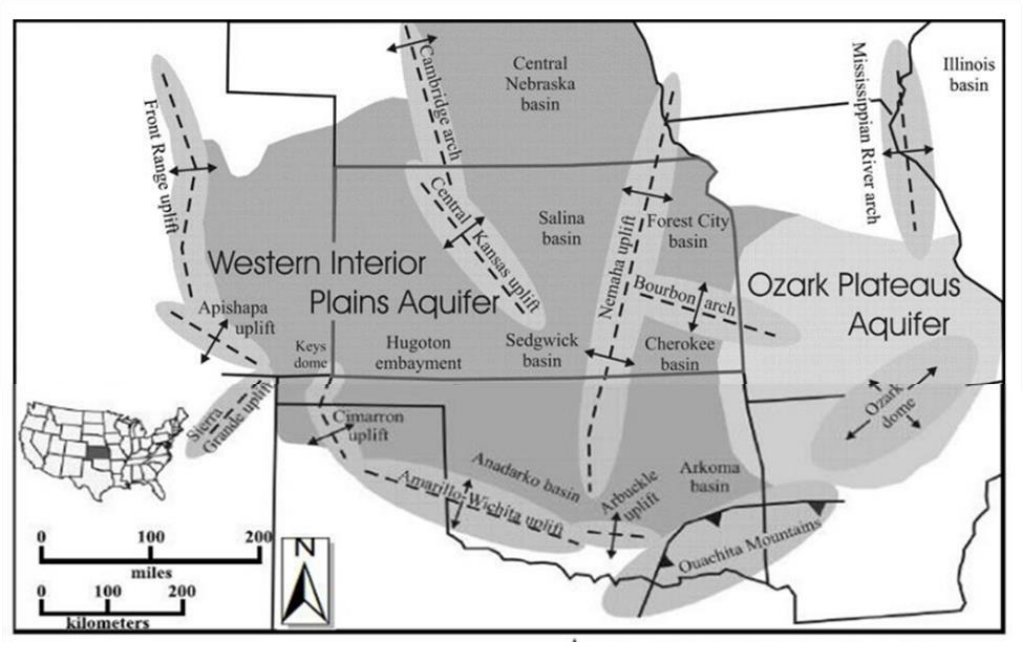

Figure 12: Map of Arbuckle Group. Modified from (Birdie, et al., Assessing Induced Seismicity Risk at the Wellington Geologic Sequestration Site, 2022)

Table 2: Arbuckle core results (Daneshfar, Hughes, & Civan, 2009)

Depth	Quartz	Calcite	Dolomite	Illite	Smectite	Kaolinite	Chlorite	Pyrite	Ortho	Oligio	Mixed	Albite	Anhydrite	Siderite
ft								*%*						
2364	0	2	94	0	0	0	0	3	0	0	1	0	0	0
2365	4	3	84	0	3	0	0	4	2	0	0	0	0	0
2367	1	1	94	2	0	1	0	0	1	0	0	0	0	0
2369	2	2	88	3	0	0	0	2	2	0	0	0	0	0
Average	2	2	90	1.25	0.75	0.25	0	2.25	1.25	0	0.25	0	0	0

Considering existing disposal wells for this analysis, the data was used to simulate CO_2 sequestration into the Arbuckle Group. Most of these wells were close to power plants, providing a room to minimize transportation costs during sequestration. The location of these wells is shown below and the summary data for these wells are shown in Table 2 below. The depth of completion for the wells was in the range of 1335 ft – 7570 ft. Permeability and average porosity in the range of 10 – 60 millidarcy, and between 7% – 18% respectively. The average property for

CO_2 sequestration across the Arbuckle Group is then presented in Table 3 below and this was used as the base case for modelling.

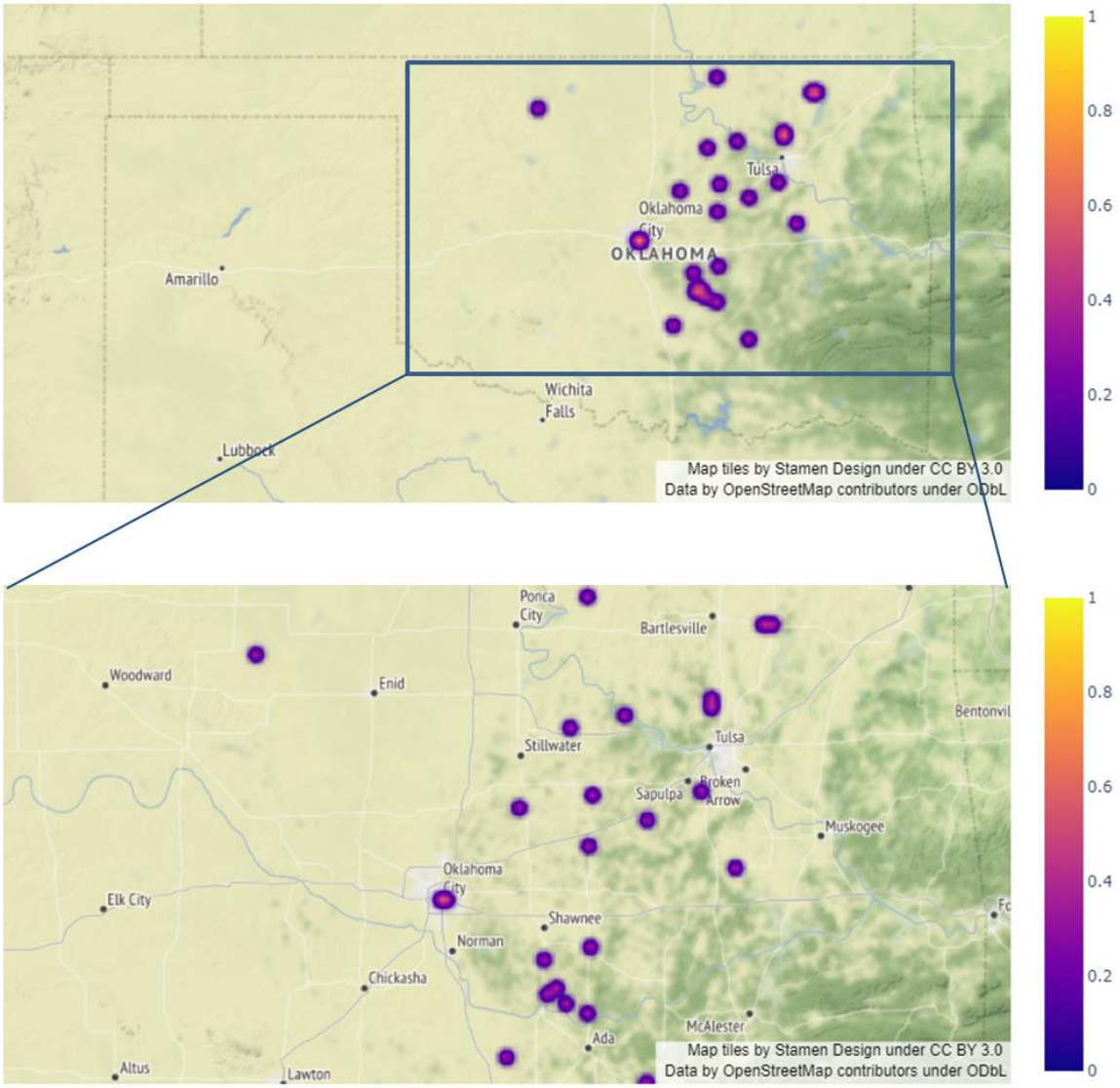

Figure 13: Location of Disposal Wells

Table 3: Disposal Wells Completion Data (Daneshfar, Hughes, & Civan, 2009)

County	API	S	T	R	D	Inj. Rate	Pressure	Treatable water base	TDS	Cl-	Perf. Top	Perf. Bottom	Porosity	K	Name	Latitude	Longitude
						bbl/d	*psi*	*ft*			*ft*	*ft*	*%*	*md*			
29	20422	27	02N	09E	8750	10000	1000	450	188890	111503	7153	8750	15	10	ARBUCKLE	34.61449	-96.3459
37	28159	34	16N	09E	4200	6000	1000	375	145500	87300	3830	4200	0	0	ARBUCKLE	35.82067	-96.343
37	75027	16	17N	12E	3060	3000	700	250	0	0	2706	3060	0	0	ARBUCKLE	35.95131	-96.0395
49	23783	18	03N	02E	4900	4500	1800	336	46200	27700	3633	4900	18	37	ARBUCKLE	34.73172	-97.1333
71	22393	8	27N	01W	3950	2000	1000	0			3872	3950			ARBUCKLE	36.83264	-96.6791
81	1441	22	17N	06E	4144	6000	600	670	0	0	3834	4144	0	0	ARBUCKLE	35.93473	-96.651
81	22309	9	14N	06E	5100	6000	1000	350	0	0	4700	4800	0	0	ARBUCKLE	35.70236	-96.6713
81	23725	11	16N	02E	7334	60000	750	680	156000	566000	5449	7334	7		ARBUCKLE	35.87629	-97.0622
105	27971	30	26N	16E	1358	3000	500	450	0	46036	1335	1355	16	0	ARBUCKLE	36.70631	-95.6386
105	23412	27	26N	15E	1506	3000	350	50			1490	1502	10	58	ARBUCKLE	36.70631	-95.6927
109	37654	1	11N	03W	7141	10000	0	850	226400	143573	6518	6818	0	0	ARBUCKLE	35.45672	-97.4685
109	35633	3	11N	03W	8835	0	0	775	0	0	7106	8835	0	0	ARBUCKLE	35.45669	-97.5039
111	22510	17	13N	14E	3872	3000	800	280	0	0	3071	3856	0	0	ARBUCKLE	35.60278	-95.8465
117	20838	17	21N	08E	2900	3000	800	550	0	0	2416	2900	0	0	ARBUCKLE	36.29674	-96.4686
117	22662	4	20N	05E	5047	12000	250	160	0	0	4055	5047	0	0	ARBUCKLE	36.23964	-96.776
125	21026	26	07N	04E	5869	5000	300	300	0	0	5012	5869	0	0	ARBUCKLE	35.05124	-96.8521
125	21057	5	06N	04E	6499	10000	0	323	0	0	5388	6499	0	0	ARBUCKLE	35.02225	-96.905
125	21934	7	08N	04E	6300	10000	500	350	0	0	5000	6300	0	0	ARBUCKLE	35.18182	-96.9227
125	22233	20	06N	05E	4654	10000	1000	0	0	0	3950	0	0	0	ARBUCKLE	34.97866	-96.7992
133	22860	4	05N	06E	5935	1000	1000	645	0	0	4355	5935	0	0	ARBUCKLE	34.9348	-96.6791
133	21631	22	09N	06E	6300	5000	300	1050	0	0	5500	6500	0	0	ARBUCKLE	35.23924	-96.6622
143	21066	24	22N	12E	2072	4000	600	350	0	0	1872	1882	0	0	ARBUCKLE	36.3729	-95.9828
143	22684	1	21N	12E	2000	7000	700	350	0	0	1850	2000	18	59	ARBUCKLE	36.32939	-95.9828

Table 4: Reservoir Properties

Parameter	**Values**	**Method**
Reservoir Depth	5034 ft	Average depth for all disposal wells
Pore pressure gradient	0.178psi/ft	Average pressure gradient for all disposal wells
Average overburden density	2.58g/cm^3	From density log of Arbuckle formation, compared with knowledge of lithology of area
Maximum injection pressure	2718 psi	Average fracture gradient in Arbuckle formation = 0.6 psi/ft from step rate test by (Birdie, Holubnyak, Watney, & Hollenbach, Methodology for Constructing Reservoir Maximum Pore Pressure Maps to Meet Class VI Constraints and Prevent Earthquakes, 2022) According UIC Class IV Requirements, the injection pressure should be less than 90% of formation fracture gradient 0.6 * 0.9 * Average Depth
Median friction coefficient	0.7	default values in the SOSAT
Standard Deviation of logarithm of fault friction coefficient	0.15	default values in the SOSAT
Maximum possible friction coefficient	1.0	Obtained from Literature by (Schulz, Müller, Röckel, & Schilling, 2020).

Table 5: Regional Stress Info Parameters

Parameter	**Values**	**Method**

Normal faulting weight	3	Stress orientations in the Arbuckle Group show SS in S-Oklahoma, and SS and NF in N-Oklahoma according to (Schulz, Müller, Röckel, & Schilling, 2020). Based on these, weighted values were assigned referenced from (Appriou, 2019).
Strike-slip faulting weight	15	Stress orientations in the Arbuckle Group show SS in S-Oklahoma, and SS and NF in N-Oklahoma according to (Schulz, Müller, Röckel, & Schilling, 2020). Based on these, weighted values were assigned referenced from (Appriou, 2019).
Thrust faulting weight	0.1	Stress orientations in the Arbuckle Group show SS in S-Oklahoma, and SS and NF in N-Oklahoma according to (Schulz, Müller, Röckel, & Schilling, 2020). Based on these, weighted values were assigned referenced from (Appriou, 2019).
K-thrust	100	default values in the SOSAT
K-SS	100	default values in the SOSAT

Table 6: Stress Measurement Parameters

Parameter	**Values**	**Method**
Mean of the minimum principal stress measurement	2870 psi	Injection pressures from mini frac tests of 15 wells were analyzed by (Schulz, Müller, Röckel, & Schilling, 2020). The average Sh gradient was 0.5525938 psi/ft.
Standard deviation of minimum principal stress measurement	220 psi	default values in the SOSAT
Minimum value of stress path coefficient	0.4	default values in the SOSAT

Minimum value of stress path coefficient	0.7	default values in the SOSAT

3.6 Seismicity in Area of Study

Areas in north central Oklahoma have experienced secondary seismicity due to injection since around 2009. Currently in the Arbuckle Group, induced seismicity is caused by two major reasons: wastewater disposal and hydraulic fracturing.

3.6.1 Wastewater Disposal

Due to the prolific nature of the oil and gas industry in Oklahoma, there is a multitude of wells and with this, a similar trend with produced water. This produced water, also called wastewater, exists underground in the rock formations, and accompanies hydrocarbon production to surface. Under the Underground Injection Control (UIC) program, which is monitored by the United States Environmental Protection Agency (EPA), Class II injection wells are used for water disposal of hydraulic fracturing fluids and produced water disposal. These account for under 10% by volume but are still a major cause of earthquakes in the Arbuckle Group because there is direct pressurization of the fluid in already existing faults and increase in stress in surrounding formations (Oklahoma Corporation Comission, 2021).

Seismicity may result from wastewater disposal into geologic formations. These activities have been observed to induce earthquakes at distances greater than10 km from the disposal site as a result of direct increase in pore (Rubinstein & Mahani, 2015). More recent research has shown that other factors such as poro-elastic stress transfer, can even result in magnitudes reaching up

to 30 km from the site of disposal or injection Goebel, 2018). Different studies have been conducted to determine if there is a relationship between Class II disposal wells and seismicity (Weingarten, Ge, Godt, Bekins, & Rubinstein, 2015); (Skoumal, Ries, Brudzinski, Barbour, & Currie, 2018); (Kolawole, et al., 2019). According to these studies, there are two major sources of fault re-activation, the increase in direct pore pressure in fault zones (McGarr & Barbour, 2017) and the pore-elastic stress changes due to proximity of faults. The Arbuckle Group lies directly above a highly fractured crystalline basement rock. According to recent research, increase in pore pressure from the point of injection and regional stress state changes across central and northern Oklahoma are the major source of induced seismicity in these areas (Walsh & Zoback, 2015); (Snee & Zoback, 2020).

3.6.2 Hydraulic Fracturing

Hydraulic fracturing is the process of injecting fluid into the formation, at pressures higher than in fracture pressure of the formation, in order to fracture the rock and allow flow of hydrocarbons. This has been used to improve productivity in Oklahoma for more than sixty years. Hydraulic fracturing also results in direct pressurization of the fluid in already existing fractures and faults and poroelastic stress transfer.

Earthquakes caused by hydraulic fracturing are usually local and often less than about 16400 ft from the point of injection. It is also less common than the regional stress changes from water injection in Class II UIC wells (Oklahoma Corporation Comission, 2021). This is because less than 10% of Oklahoma's cumulative disposed fluids are from HF on average (Murray, 2013). Recent studies show that about 7% of hydraulic fracturing wells that were completed from late 2016 to middle of 2019 ensued earthquakes with magnitude greater than 2 (M2.0+) (Shemeta J.

E., Brooks, & Lord, 2019). The seismicity that is induced by hydraulic fracturing is very variable and highly depends on the geology of the subsurface, hence, pre-existing fracture systems and faults are a major factor.

3.6.3 Data

Previous studies have some to a consensus that wastewater injection into the Arbuckle Group, one of the deepest formations in Oklahoma state, translates to a high probability of induced seismicity with large magnitudes (Walsh & Zoback, 2015). Before 2009, the magnitude of earthquakes in the Arbuckle Group were less than M3.0+ earthquake yearly. In about 2015, the state of Oklahoma reached a peak where there were more than 900 earthquakes with magnitudes greater than M3.0+. After this, seismicity in Oklahoma has continued to decline mostly due to the intentional efforts implemented by the Oklahoma Corporation Commission (OCC) and potential stakeholders year after year such installing more seismicity monitors. Recent data has shown that in December 2020 Oklahoma recorded 37 magnitudes M3.0+ earthquakes (Oklahoma Corporation Comission, 2021).

Injection CO_2, although a lighter fluid than produced water, it is still capable of introducing this behavior, hence, it is important to understand the existing seismicity in the area of study and then predict the probability of seismicity during CO_2 sequestration.

3.6.4 Cluster Analysis

Cluster analysis was used to demonstrate the seismicity in the area using two datasets. The first dataset included the records of Oklahoma's active saltwater injection wells as of September 2017 which was gathered from Oklahoma Corporate Commission. The second dataset was a list of all

the earthquakes in the Arbuckle Group since 1977 and was gathered from the United States Geological Survey. Clustering is an approach where a set of parameters of a particular attribute are grouped based on the similarity the object has to each other as opposed to the similarity with other parameters in a different cluster. Aside from being an important part of exploratory data analysis and statistical data analysis, it is also an approach to unsupervised machine learning. It has been used in many applications such as bioinformatics, data compression, pattern recognition, information retrieval, and computer graphics (Wikipedia, Cluster analysis, 2022).

There are different clustering techniques, but for this work the K-Means algorithm which is a partitional clustering technique. K-Means partitions the data into k distinct clusters where each data point in the data belongs to the cluster that has the cluster centroid or closest mean to it (Wikipedia, Cluster analysis, 2022).

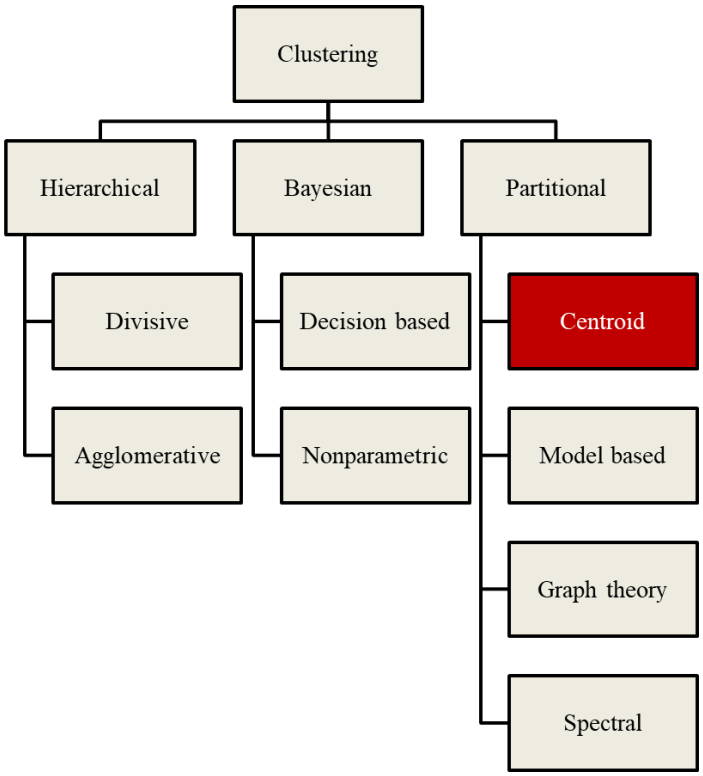

Figure 14: Clustering algorithms. Modified from (Wikipedia, Cluster analysis, 2022)

K-Means is a very common unsupervised clustering algorithm because it is very intuitive and simple to use. It is an unsupervised clustering algorithm because the number of clusters present in the data, similar data points or dissimilar data points are not known. Based on the algorithm, the clusters containing points similar to other points are grouped within the same cluster and dissimilar datapoints grouped in other clusters.

CHAPTER 4: Results and Discussion

4.1 Introduction

The result in this chapter first shows the trend in the seismicity of the area. A Bayesian technique is then used to show a probability model of activating a critically oriented fault in the Arbuckle Group based on available data.

4.2 Seismicity in Area

The plot below shows the seismic events around the Arbuckle Group. The seismic events were obtained from the US Geological Survey. They were distributed around the Arbuckle group and had attributes like the location, longitude and latitude of the event, the depth of seismic event, the magnitude, and the source. From the plot most of the events are below M4.0 in magnitude. The bulk of the seismicity events are also concentrated around central Oklahoma. To further utilize the data appropriately, several data cleaning techniques were employed. To handle the missing data in the dataset, all the rows with more than 20% missing values as shown in missingness map below were all dropped. The remaining missing values for the attributes like the horizontal error and depth error were computed using the average of the other properties. This did not skew the dataset as the location which was the attribute clustered did not any have missing values.

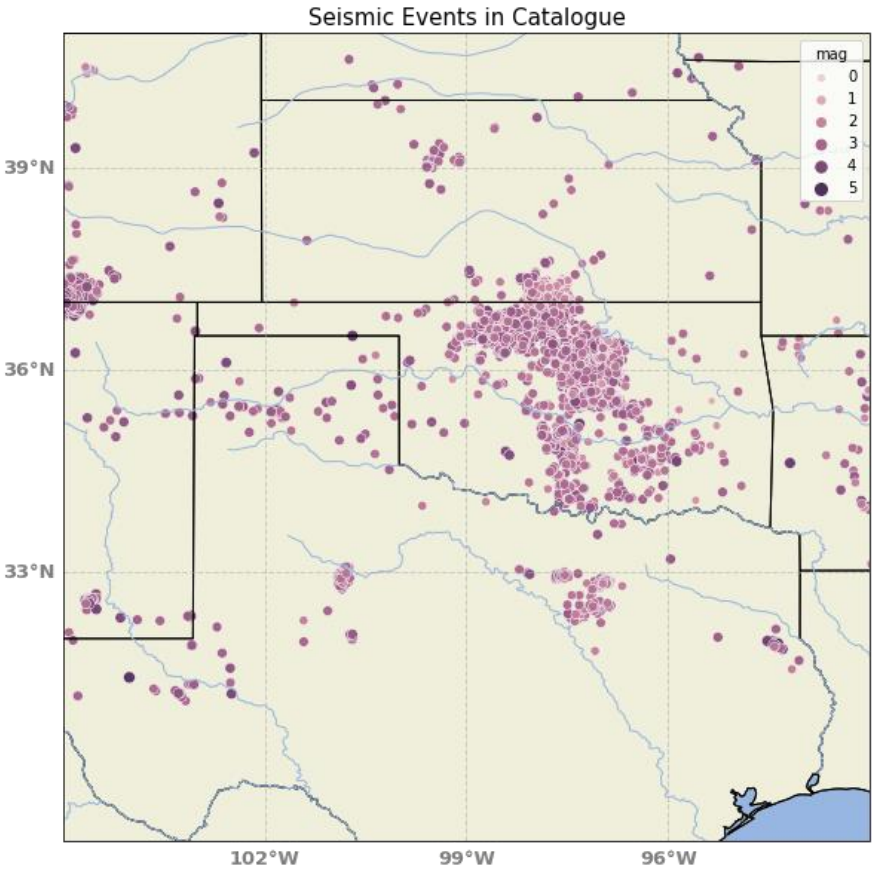

Figure 15: Seismic Events in Catalogue

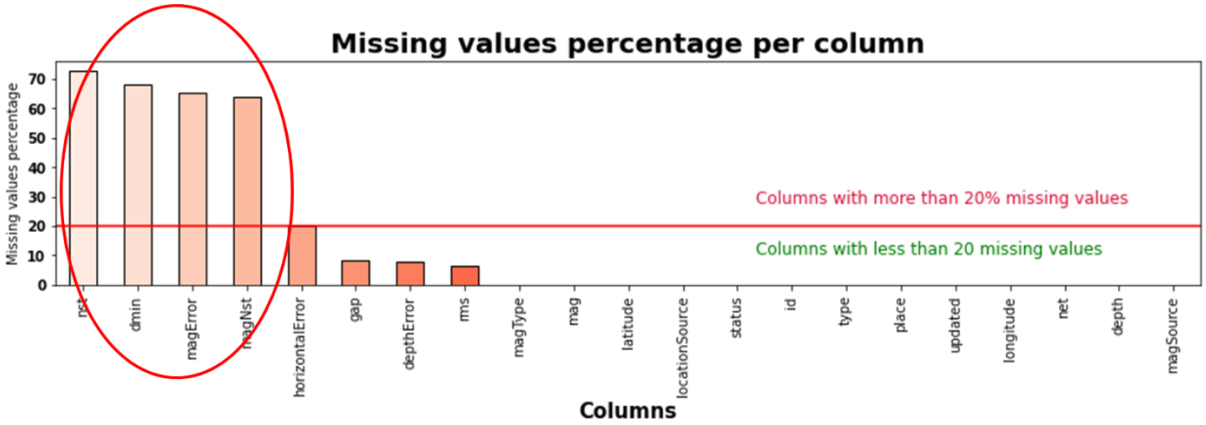

Figure 16: Missingness map for seismic data showing attributes with more than 20% missing value

After performing the data cleaning, the data was then explored to understand the seismicity in the area. The figure below shows the number of seismic events from 1975 to date. From the plot, it is observed that the seismicity increased significantly after 2008. Higher magnitudes were also attained after this time.

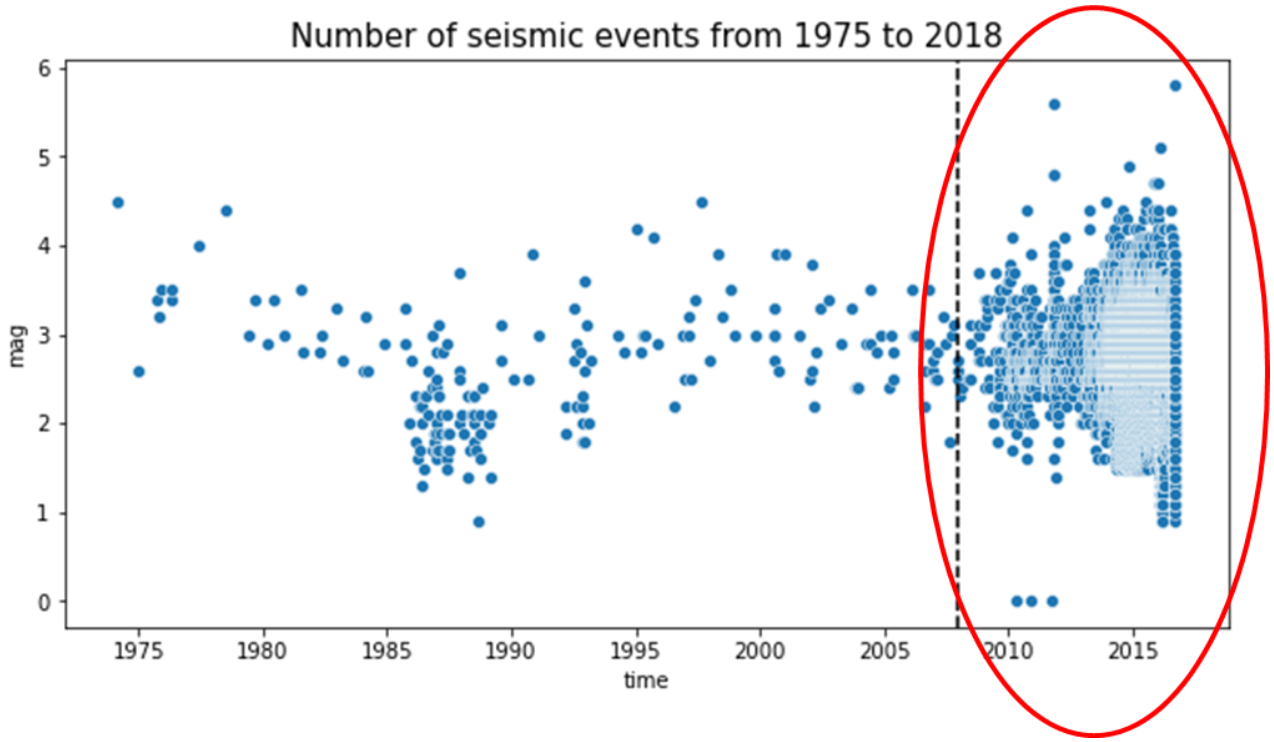

Figure 17: Number of seismic events from 1975 to 2018

After this, the earthquakes were then grouped into clusters based on their location, and the goal was to see if these clusters matched the clusters of injection wells around the Arbuckle group. The first step was to determine the number of optimal clusters (k) for clustering the earthquakes. Clusters should be between 10 and 20 based on the different locations of the earthquakes.

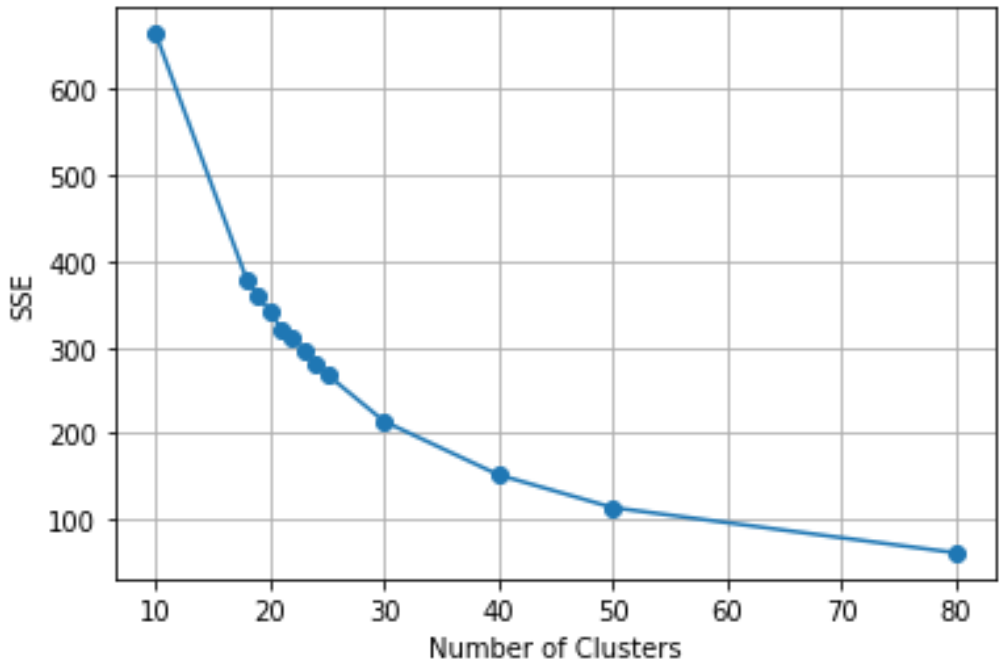

Figure 18: K for Clustering Earthquakes

The clusters of earthquakes identified from the data are shown in the figure below. These clusters would then be compared to the clusters obtained in the injection data to check for a relationship.

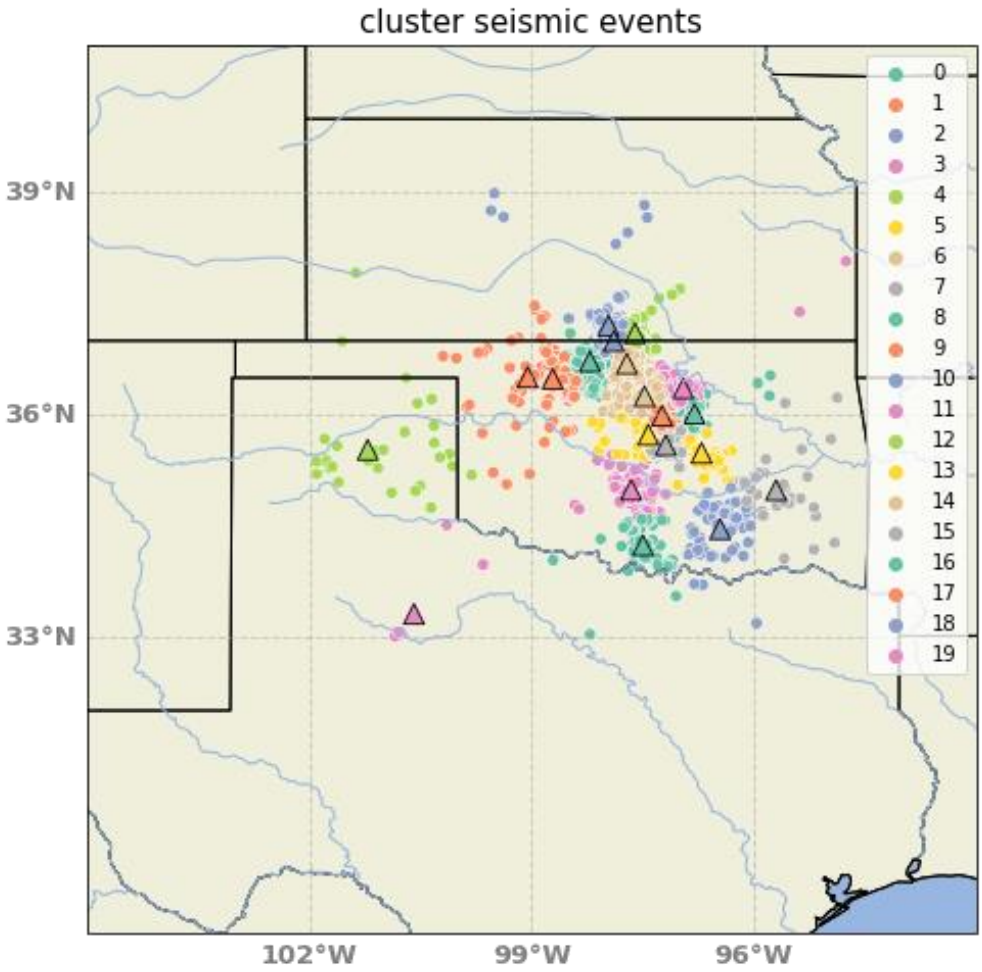

Figure 19: Cluster analysis of seismic events

Injection Data

The injection wells were obtained from the Oklahoma Corporation Commission. They were distributed around Oklahoma and contained attributes such as the well location and identification, the injection pressures and volumes, and so on.

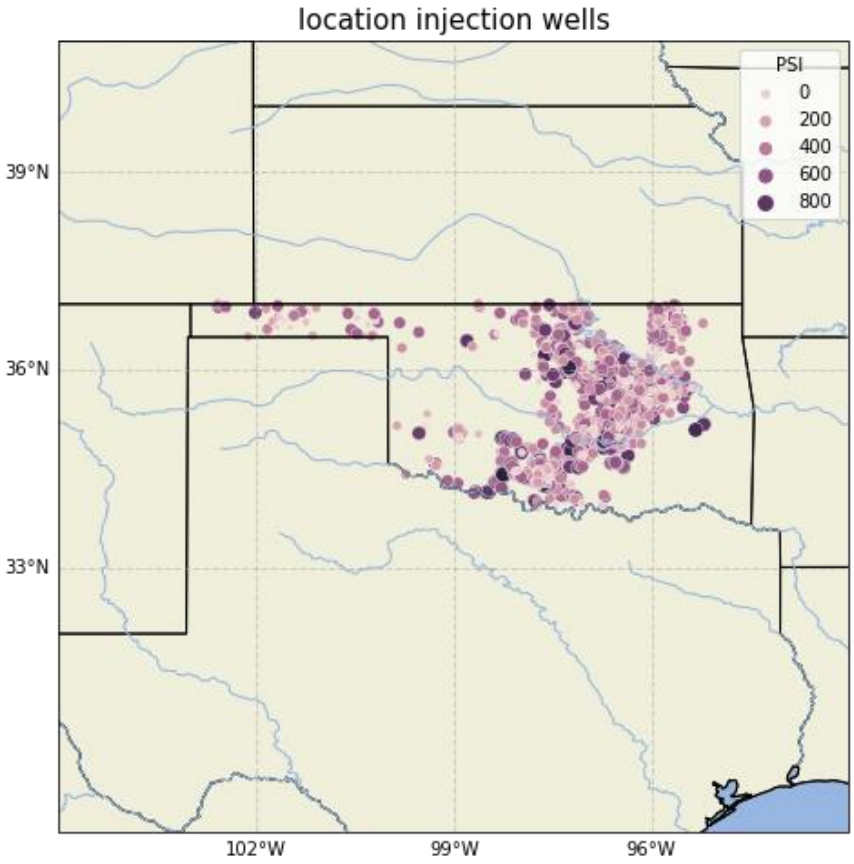

Figure 20: Injection wells in catalogue

The first step in the injection data is to clean the data, by checking for missing data, imputing it, as well as handling possible outliers. Here, unknown attributes highlighted below were dropped. The remaining missing values for the attributes like the volume in bbls and pressure in psi were computed using the average of the other properties. This did not skew the dataset as the location which was the attribute clustered did not any have missing values.

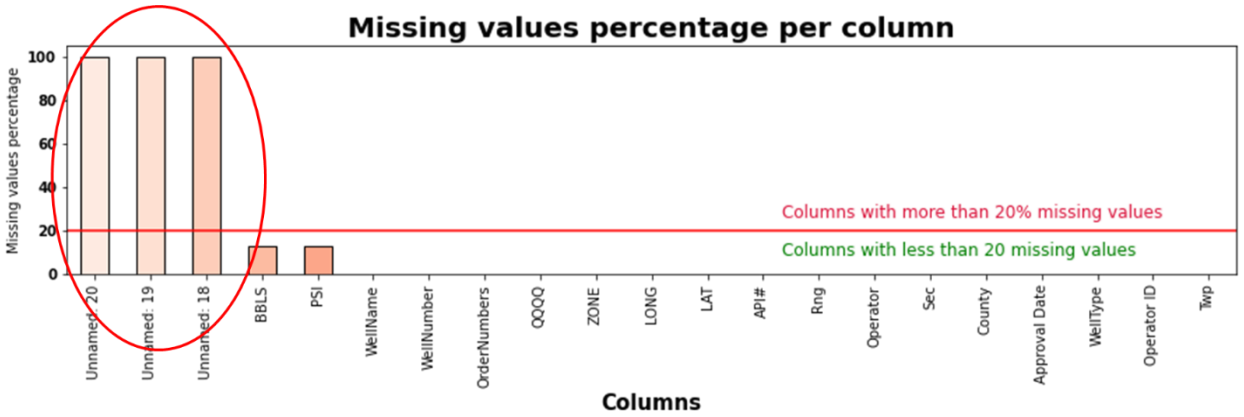

Figure 21: Missingness map for seismic data showing attributes with more than 20% missing value

After this, the injection wells were then grouped in clusters, and the goal was to see if these clusters matched the clusters of seismicity obtained above. The first step was to determine the number of optimal clusters (k) for clustering the wells. Clusters should be between 10 and 20 based on the different locations of the injection wells.

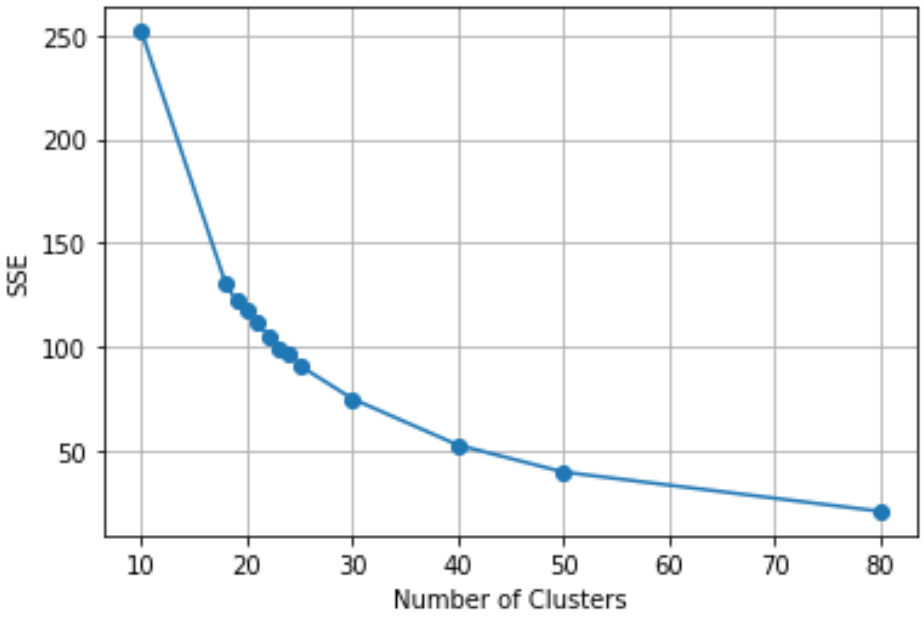

Figure 22: K for Clustering Wells

Comparing the clusters for the seismicity events to the cluster of the injection wells, there is a direct relationship as shown in the figure below. The cluster analysis shows there is an overlap between areas with injection wells and seismic events. This emphasizes that injecting fluid into the Arbuckle Group has a causation on the seismicity events. To achieve optimal carbon sequestration, which is the injection of CO_2 into the formation, there is need to determine the probability of inducing seismicity by activating a critically oriented fault.

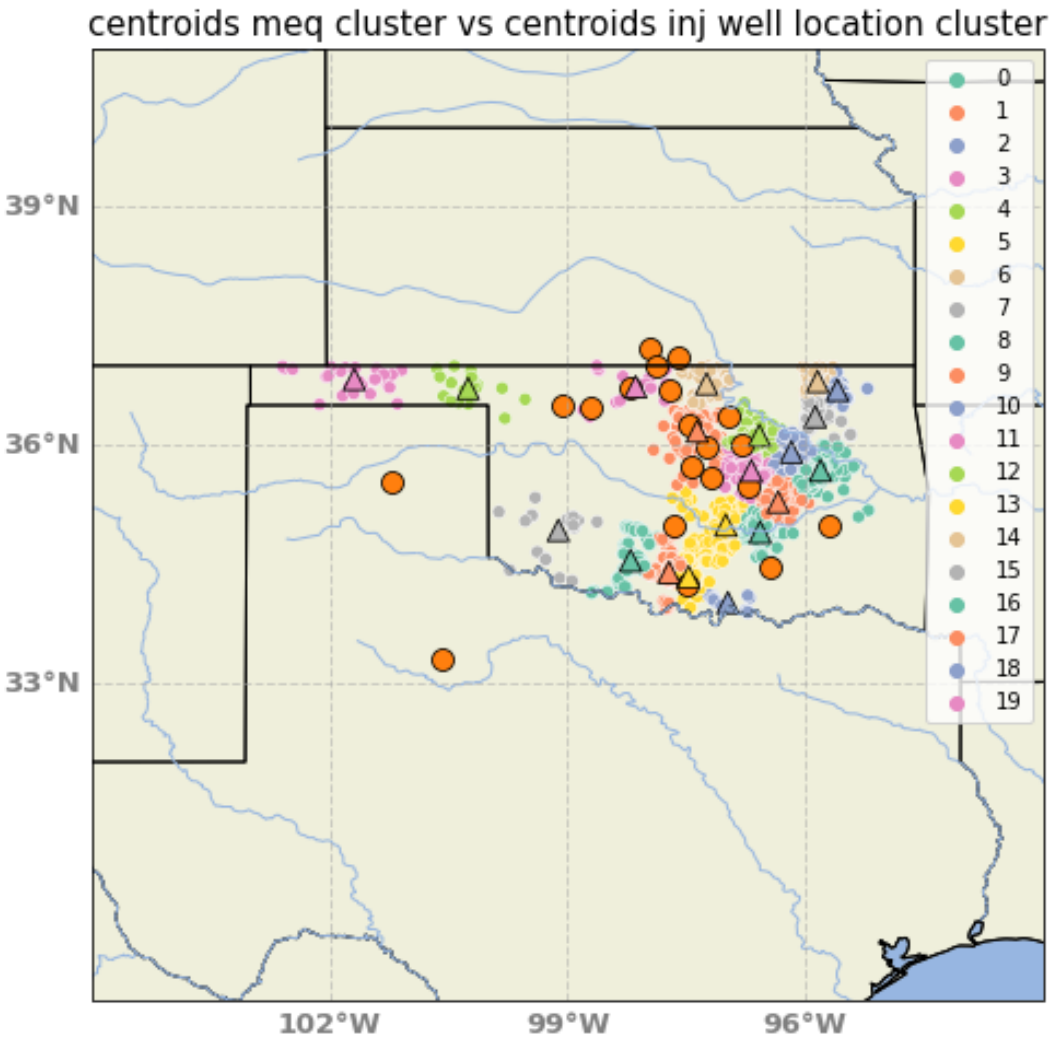

Figure 23: Cluster analysis of seismic events vs injection wells

4.3 Probability Model

After implementing the Bayesian model with the aid of the SOSAT tool, the figure below shows the probability plot of the friction coefficient, which serves as an input to calculating the risk of failure. For the model a lognormal distribution with a mean of 0.7 and standard deviation of 0.15 was chosen for the probability plot of the friction coefficient, which serves as an input to calculating the risk of failure. For each additional scenario run in the sensitivity analysis, the shape of this plot would change. The sensitivity analysis is done to identify the different features that have multiple predictor dependence on the geomechanical risk.

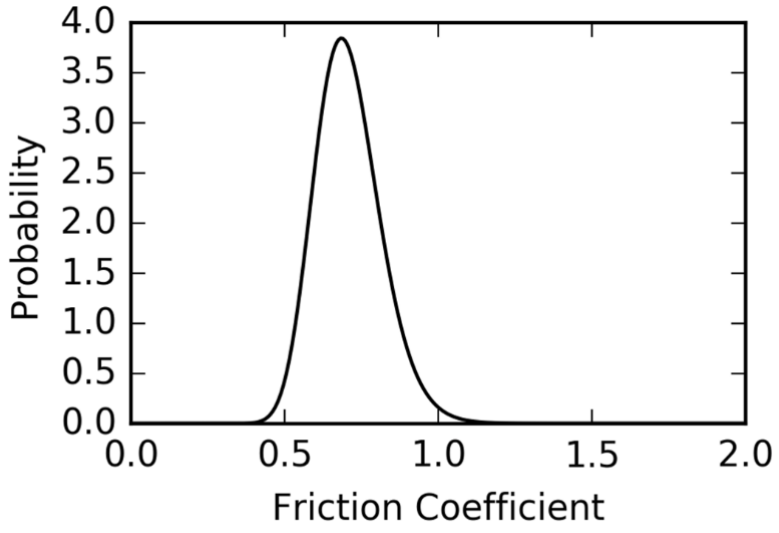

Figure 24: Probability plot of the friction coefficient

The analysis then begins with the posterior assumption that all the states of stress where the maximum horizontal stress is greater than the minimum horizontal stress ($\sigma H > \sigma h$), with both of them being compressive has an equal probability, as distribution shown in the figure below.

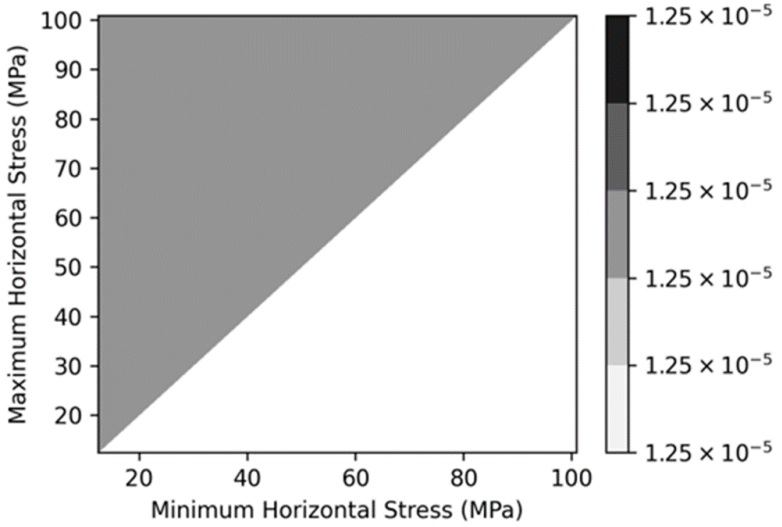

Figure 25: Assumption that all stresses are normal and have equal probabilities

The probability distribution of regional stress state information reflects that the region is mostly Strike Slip and Normal Faulting.

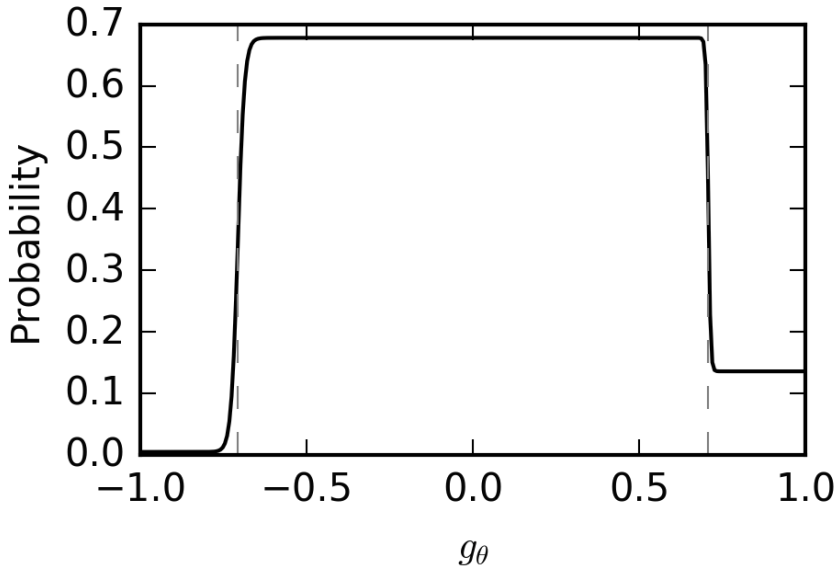

Figure 26: Probability distribution of regional stress state information

The frictional constraint which asserts that the stress cannot be larger than the frictional strength of pervasive faults and fractures is shown below. The plot shows that the minimum horizontal stress is better constrained than the maximum horizontal stress, there is considerable uncertainty

in the maximum horizontal stress, hence the assumption that both stress state holds equal probability no longer holds. The degree of uncertainty in the maximum horizontal stress ranges from 39MPa to 67 MPa. The shape of this plot can also change for each additional scenario run in the sensitivity analysis, based on the different conditions defined.

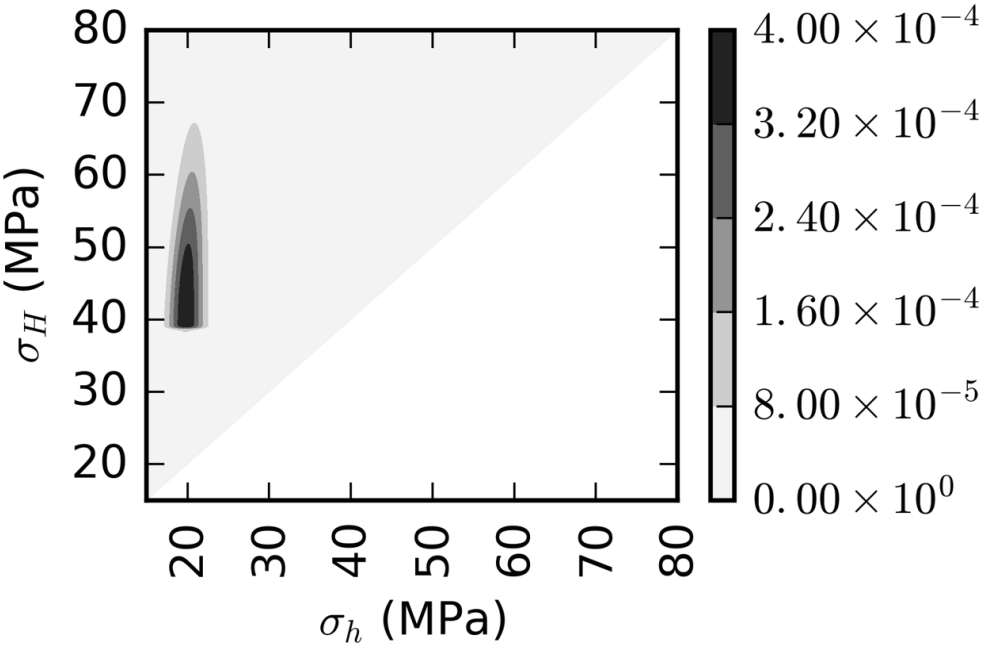

Figure 27: Posterior stress distribution plot

The next plot shows the risk or probability of activating a critically oriented fault or the shear failure probability for the given reservoir base case parameters. The results show that there is a 24% probability that it is critically stressed at initial pressures, and this increases up to 63% when the defined maximum injection pressure is attained.

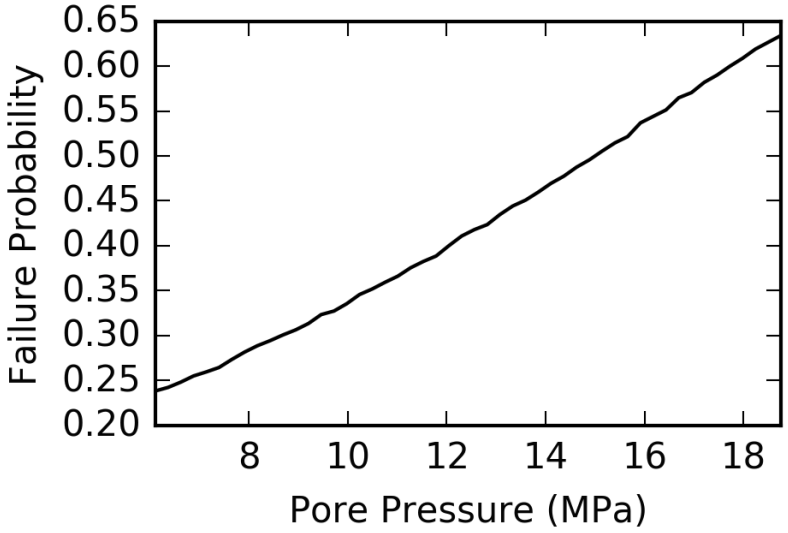

Figure 28: Probability of inducing seismicity on a critically oriented fault

4.4 Sensitivity Analysis

Sensitivity analysis was carried out on the parameters set as default in SOSAT to understand how they affected the risk of seismicity. The friction coefficient (μ) and maximum stress path coefficient (max Γh) were sensitized on.

Strike-slip and normal faulting regime

A strike-slip and normal faulting regime was first considered in figures 29 to 35. A lower friction coefficient resulted in a lower uncertainty range in maximum horizontal stresses, but higher risk of seismicity risk as shown in figures 29 to 31. Decreasing the coefficient of friction increases the probability of inducing shear failure.

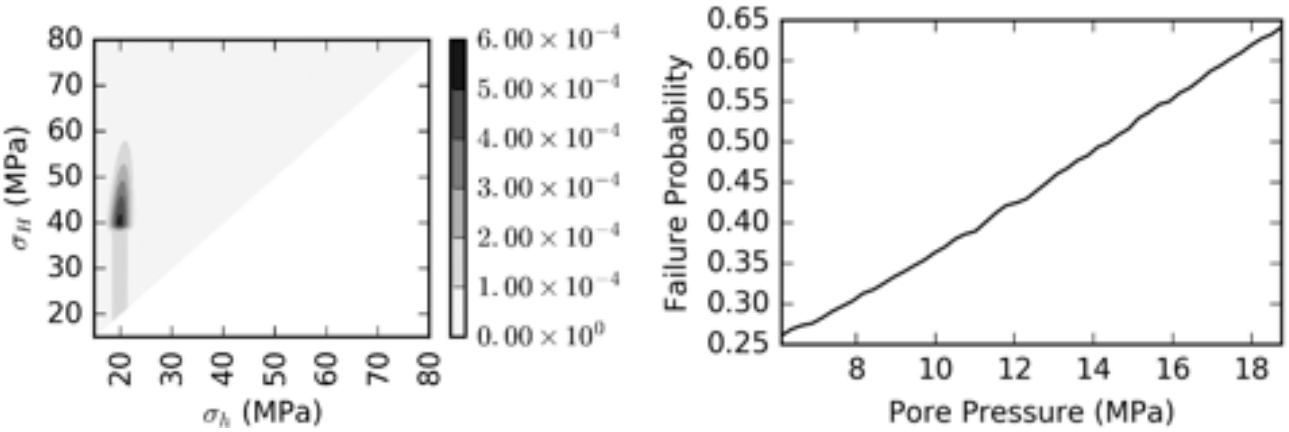

Figure 29: $\mu = 0.6$, max $\Gamma h = 0.7$

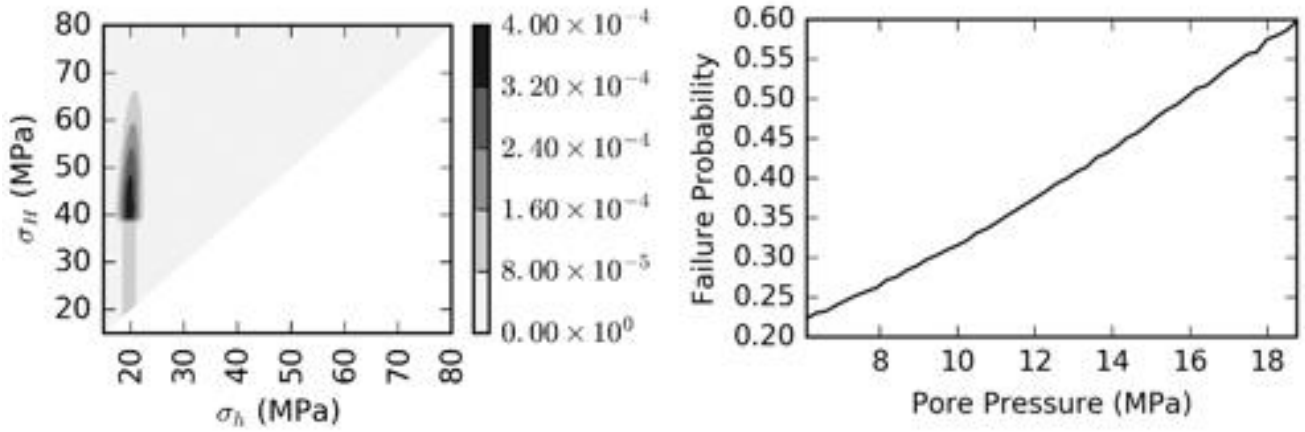

Figure 30: $\mu = 0.7$, max $\Gamma h = 0.7$

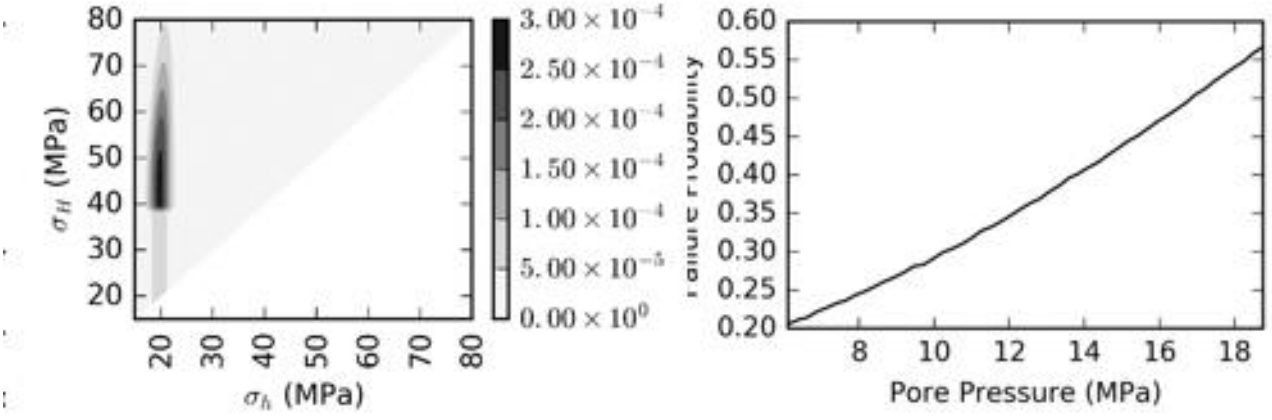

Figure 31: $\mu = 0.8$, max $\Gamma h = 0.7$

Similarly, the range of values determined for the stress path coefficient (max Γh) has a significant effect on the probability of fault activation – comparing figures 29 and 32, 30 and 33, and 31 and 34 – but not on the uncertainties observed in the maximum horizontal stresses.

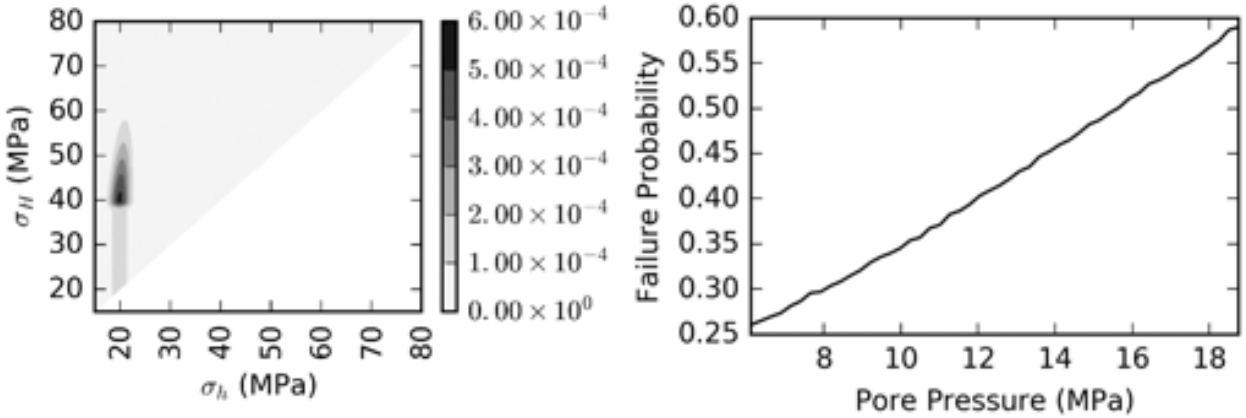

Figure 32: μ = 0.6, max Γh = 0.8

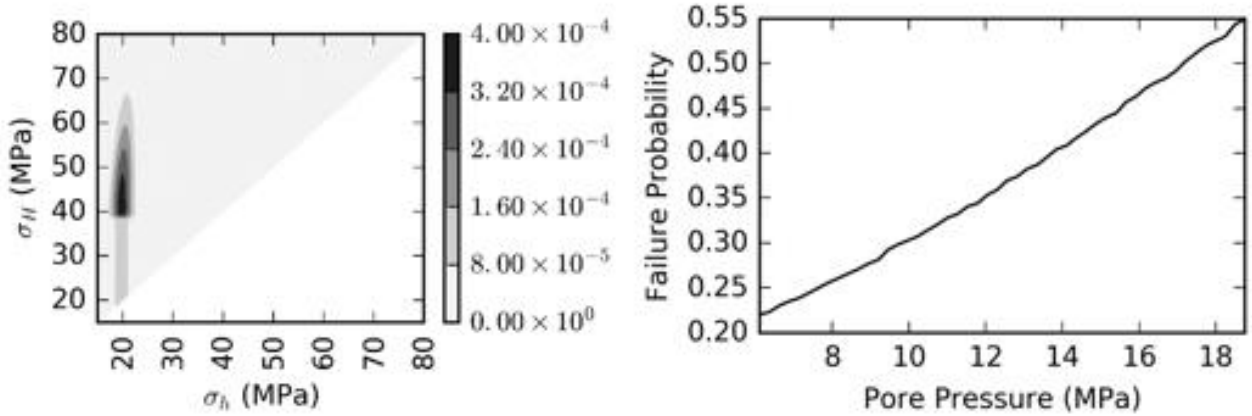

Figure 33: μ = 0.7, max Γh = 0.8

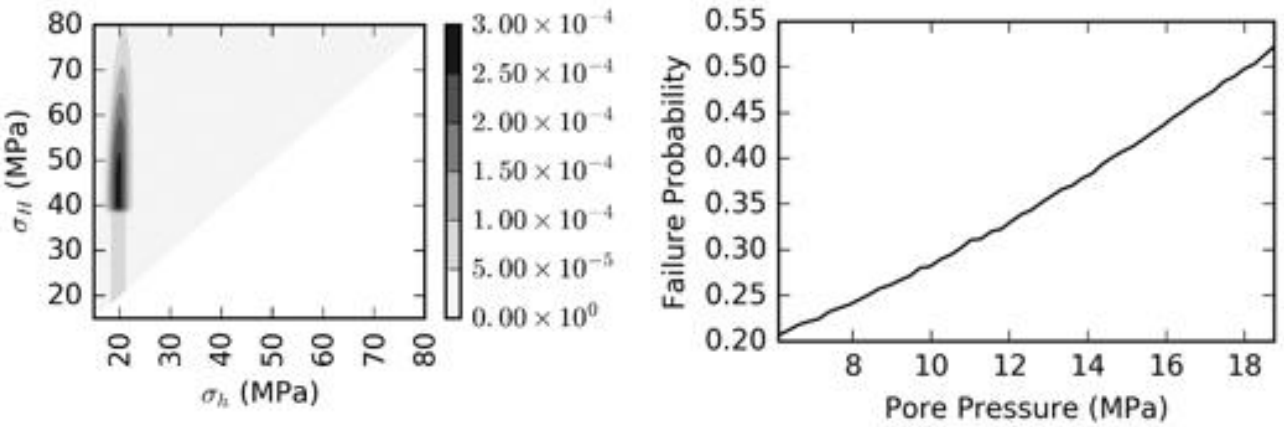

Figure 34: μ = 0.8, max Γh = 0.8

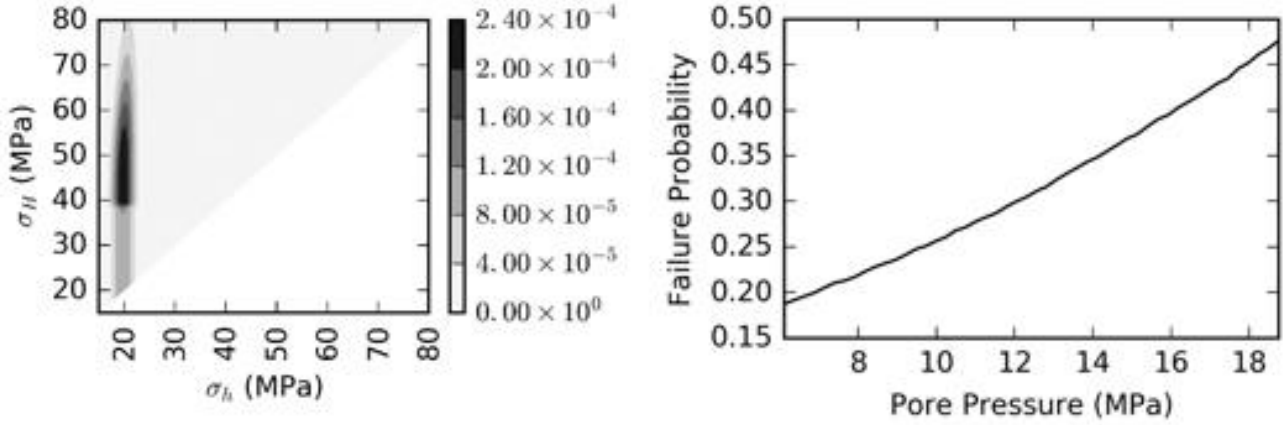

Figure 35: μ = 0.7, max Γh = 0.8, NF = 5

Pure strike-slip regime

The next regime considered was a pure strike-slip regime in figures 36 to 38. The results show that the chosen regional stress state has an effect on the risk of seismicity. Seismicity risk was higher in the pure strike-slip regime in comparison to the strike-slip faulting with normal faulting regime.

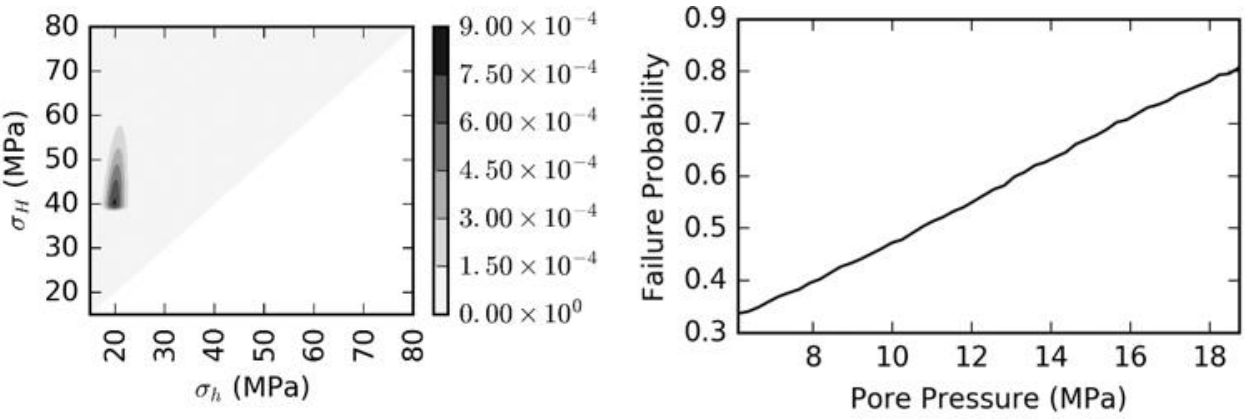

Figure 36: μ = 0.6, max Γh = 0.7

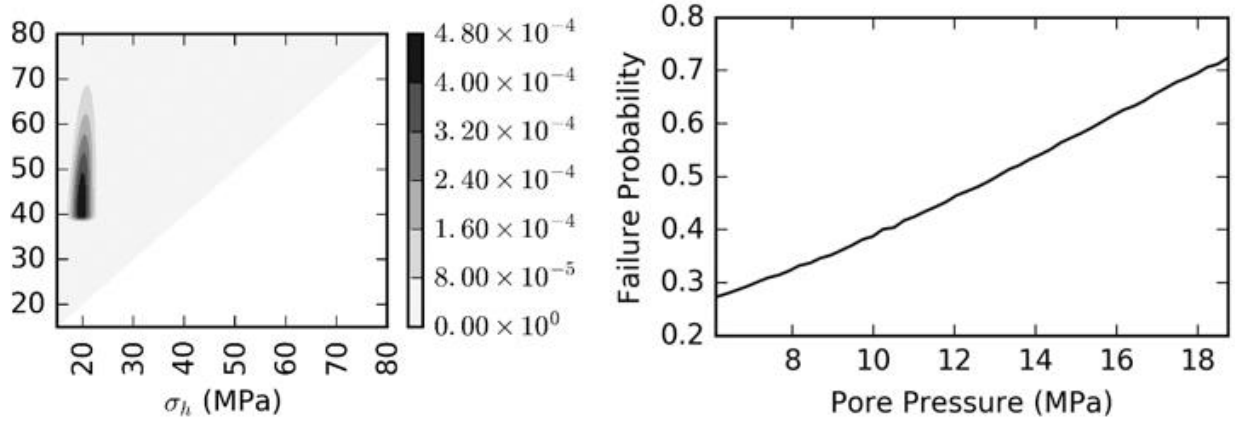

Figure 37: μ = 0.7, max Γh = 0.7

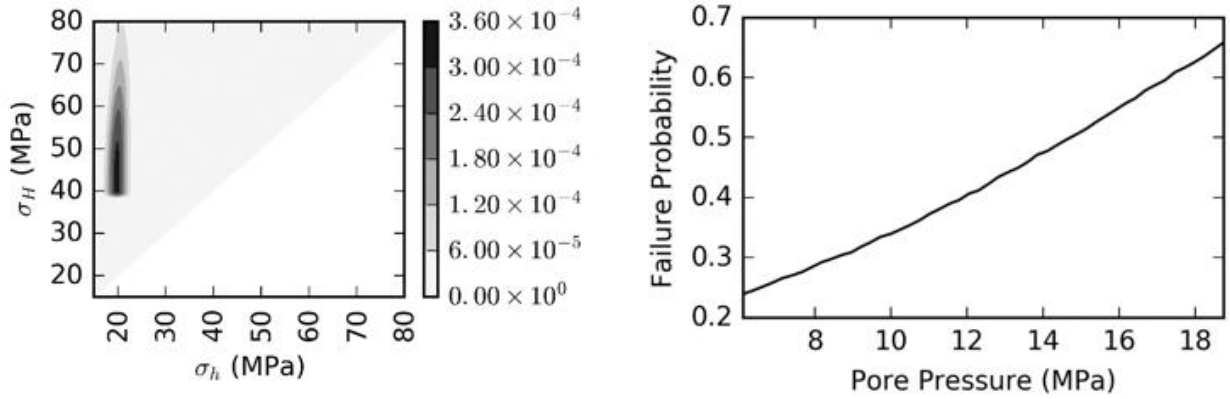

Figure 38: μ = 0.8, max Γh = 0.7

Comparing the performance of the different models, the model closest to reality from data obtained from (Birdie, et al., Assessing Induced Seismicity Risk at the Wellington Geologic Sequestration Site, 2022) was chosen as highlighted in the table below for further analysis.

Table 7: Sensitivity Analysis Summary

Case name	Definition	NF	SS	TF	μ	σ	minΓh	maxΓh	prob
SNA	Strike Slip + Normal Faulting	3	10	0.1	0.7	0.15	0.4	0.7	0.24
SNB	Strike Slip + Normal Faulting	3	10	0.1	0.6	0.15	0.4	0.7	0.26
SNC	**Strike Slip + Normal Faulting**	**3**	**10**	**0.1**	**0.8**	**0.15**	**0.4**	**0.7**	**0.2**
SND	Strike Slip + Normal Faulting	3	10	0.1	0.7	0.15	0.4	0.8	0.23
SNE	Strike Slip + Normal Faulting	3	10	0.1	0.6	0.15	0.4	0.8	0.26
SNF	Strike Slip + Normal Faulting	3	10	0.1	0.8	0.15	0.4	0.8	0.21
SNG	Strike Slip + Normal Faulting	5	10	0.1	0.8	0.15	0.4	0.8	0.18
SSA	Strike Slip	0.1	15	0.1	0.7	0.15	0.4	0.7	0.28
SSB	Strike Slip	0.1	15	0.1	0.6	0.15	0.4	0.7	0.35
SSC	Strike Slip	0.1	15	0.1	0.8	0.15	0.4	0.7	0.245
SSD	Strike Slip	0.1	15	0.1	0.7	0.15	0.4	0.8	0.28
SSE	Strike Slip	0.1	15	0.1	0.6	0.15	0.4	0.8	0.34
SSF	Strike Slip	0.1	15	0.1	0.8	0.15	0.4	0.8	0.24
SSG	Strike Slip	5	15	0.1	0.8	0.15	0.4	0.8	0.2

Different reservoir properties shown in table 8 below, were also applied to see how they affect the seismicity risk.

Table 8: Reservoir Parameters Sensitivity Summary

Depth (ft)	**Overburden gradient (*g/cm^3*)**	**Max Injection Pressure (psi)**	**Pore pressure gradient (psi/ft)**	**Mean of Min Principal Stress (psi)**
5034	2.58	2718.36	0.17586	2870
1358	2.58	2718.36	0.366819	750
9078	2.58	2718.36	0.242344	5016
5034	2.37	2718.36	0.17586	2870
5034	2.87	2718.36	0.17586	2870

The first parameter sensitized on was the depth. A range of depths from the disposal wells across the Arbuckle formation shown in table 3 was sensitized to evaluate how variation in depth affected seismicity risks. The bottom range chosen was 1358ft shown in figure 39 and the top range was 9078ft shown in figure 40. From the results in the plots, at deeper depth there is a smaller incremental change in risk with increase in depth. Observing the data distribution in table 3, most wells are not very deep and are around the average case of the base case. This suggests depth should be a consideration when designing GCS projects in the Arbuckle formation so as to minimize changes in induced risk with pressure.

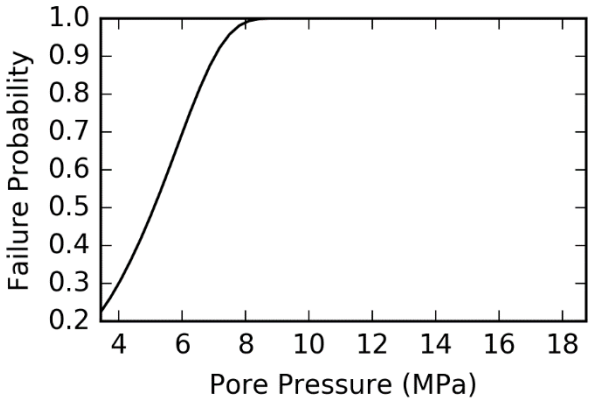

Figure 39: Depth of 1335 ft

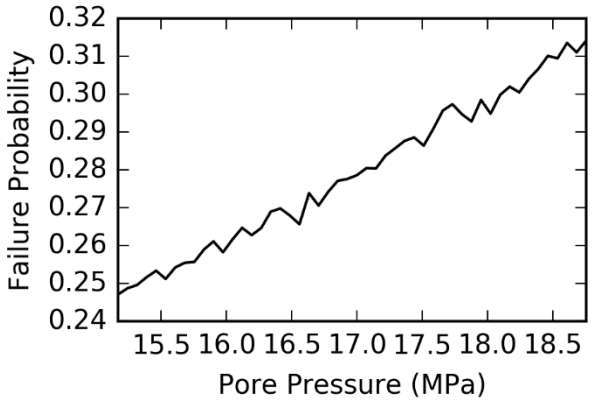

Figure 40: Depth of 7570 ft

The final analysis for this work is conducted on the overburden gradient. From the plots below, an increase in the overburden gradient slightly reduced the seismicity risks in comparison to the other reservoir properties. Overburden gradient of 1.02psi/ft and 1.24psi/ft were considered in this analysis.

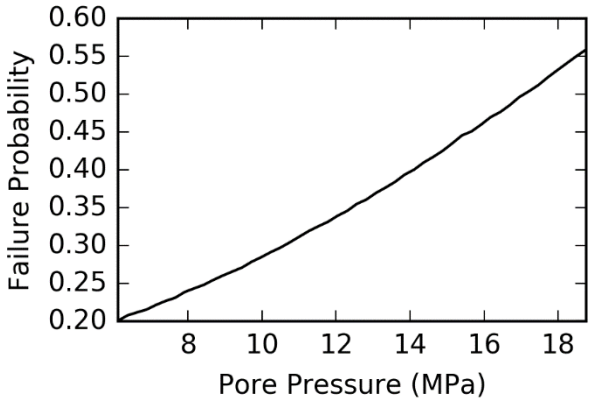

Figure 41: Overburden gradient of 1.02psi/ft

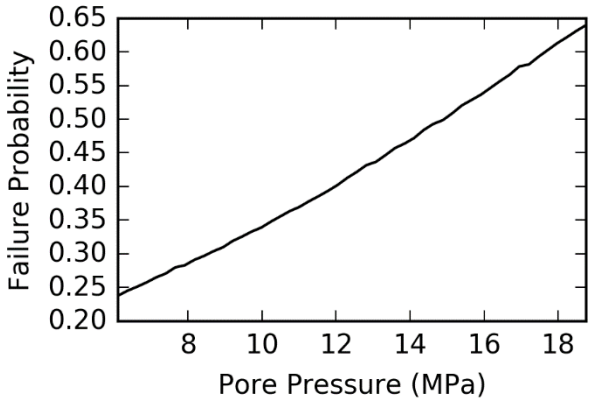

Figure 42: Overburden gradient of 1.24psi/ft

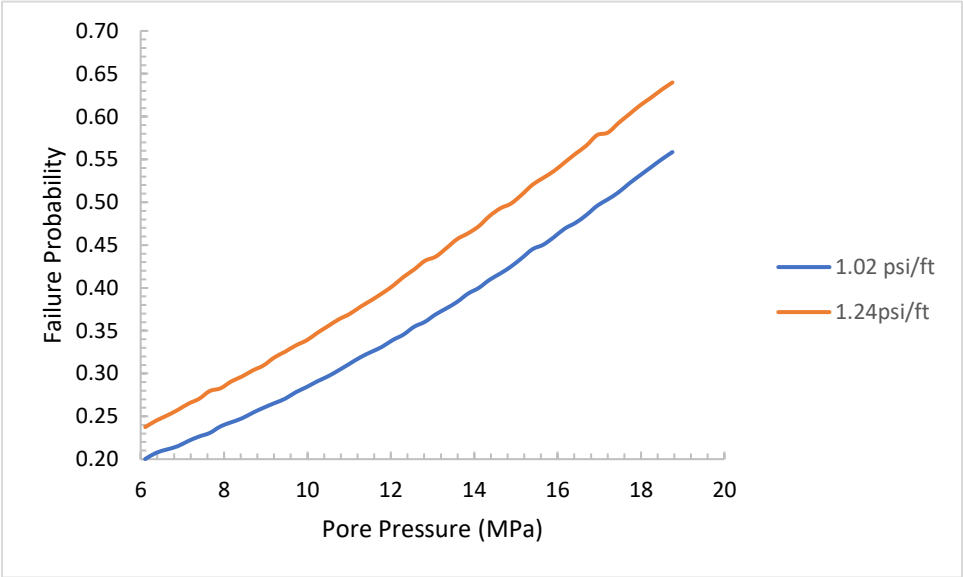

Figure 43: Comparison of overburden gradient

Based on these results, it is observed that the minimum injection pressure had a multiple predictor dependence on the risk level observed in the formation.

4.5 Site Specific Stress Data

Site specific stress data obtained from the Arbuckle Group in Kansas state was tested on the methodology. The data was taken from a pilot project at the Wellington site in south-central Kansas sponsored by the Department of Energy (DOE). The Data was obtained from (Birdie, et al., Assessing Induced Seismicity Risk at the Wellington Geologic Sequestration Site, 2022).

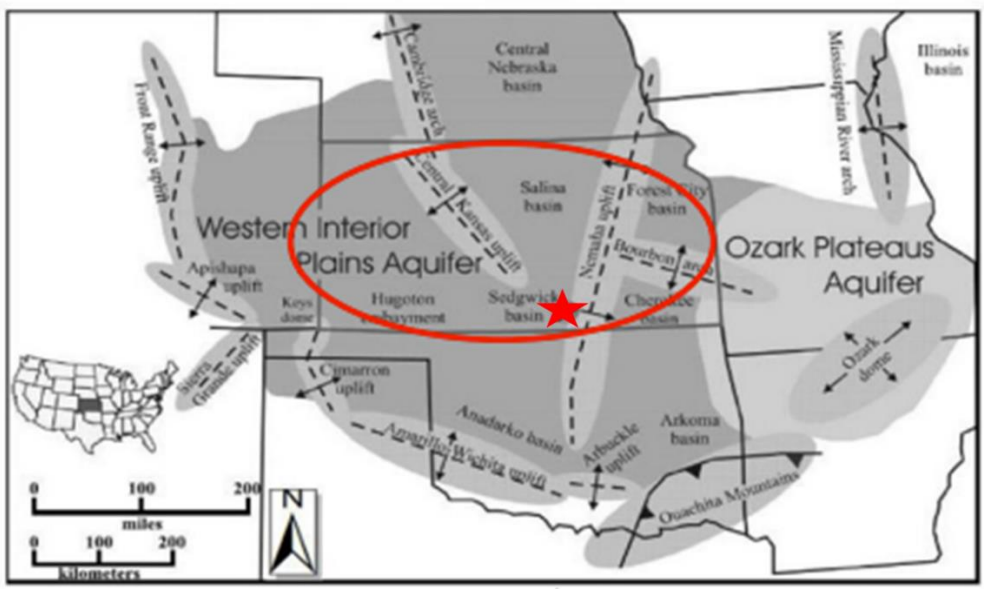

Figure 44: Map of Wellington Site in the Arbuckle Group. Modified from (Birdie, et al., Assessing Induced Seismicity Risk at the Wellington Geologic Sequestration Site, 2022)

Kansas was historically considered a seismically benign region, however, there has been an increasing number of earthquakes since 2014. This is due to an increase in the quantity of water disposal in the Arbuckle aquifer as a result of the oil and gas operations in the area. To commence CO_2 injection at the Wellington site, the US EPA, as part of the permitting process,

required an analysis to show that the injection of CO_2 into the formation would not induce seismicity. This became particularly eminent when an 8,00ft long fault was found near the injection site (Birdie, et al., Assessing Induced Seismicity Risk at the Wellington Geologic Sequestration Site, 2022).

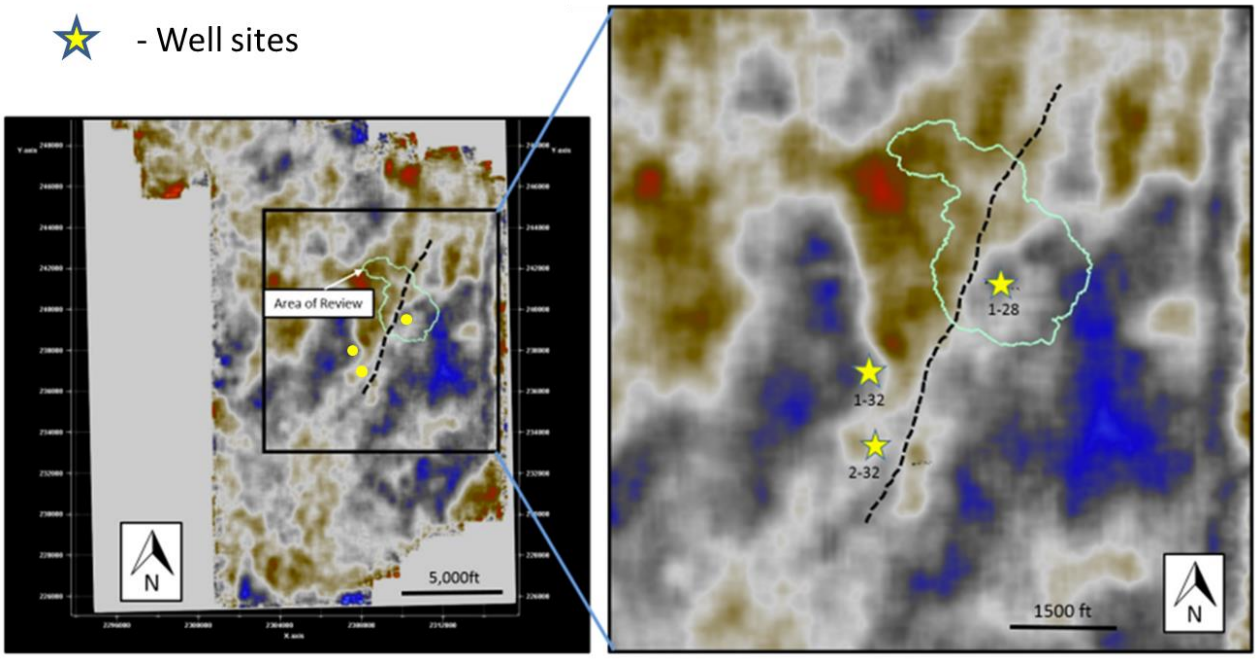

Figure 45: 8000ft Long Fault in Wellington Site. Modified from (Birdie, et al., Assessing Induced Seismicity Risk at the Wellington Geologic Sequestration Site, 2022)

The data for the model is shown in the tables below.

Table 9: Site Reservoir properties

Parameter	**Values**	**Method**
Reservoir Depth	4980ft	Injection depth
Pore pressure gradient	0.42psi/ft	Measured pressure gradient at KGS 1-32 and KGS 1-28

Average overburden density	1.12psi/ft	From density log of Arbuckle formation, compared with knowledge of lithology of area
Maximum injection pressure	2690 psi	Average fracture gradient in Arbuckle formation = 0.6 psi/ft According UIC Class IV Requirements, the injection pressure should be less than 90% of formation gradient 0.6 * 0.9 * Average Depth
Median friction coefficient	0.8	derived from 3-D stress analysis tress envelope
Standard Deviation of logarithm of fault friction coefficient	0.15	default values in the SOSAT
Maximum possible friction coefficient	1.0	Obtained from Literature by Schulz et al.

Table 10: Site Regional Stress Info Parameters

Parameter	**Values**	**Method**
Normal faulting weight	0.1	Stress orientations from regional fault in Kansas and Drilling induced fractures from well logs at the Wellington site show SS orientation (Birdie, et al., Assessing Induced Seismicity Risk at the Wellington Geologic Sequestration Site, 2022). Based on these weighted values were assigned.
Strike-slip faulting weight	15	Wellington site show SS orientation. Based on these weighted values were assigned. (Birdie, et al., Assessing Induced Seismicity Risk at the Wellington Geologic Sequestration Site, 2022). Based on these weighted values were assigned.

Thrust faulting weight	0.1	Wellington site show SS orientation. Based on these weighted values were assigned. (Birdie, et al., Assessing Induced Seismicity Risk at the Wellington Geologic Sequestration Site, 2022). Based on these weighted values were assigned.
K-thrust	100	default values in the SOSAT
K-SS	100	default values in the SOSAT

Table 11: Site Stress Measurement Parameters

Parameter	**Values**	**Method**
Mean of the minimum principal stress measurement	2887 psi	A pulse test, which is a variant of a leak-off test was conducted (Birdie, et al., Assessing Induced Seismicity Risk at the Wellington Geologic Sequestration Site, 2022)
Standard deviation of minimum principal stress measurement	220 psi	default values in the SOSAT
Minimum value of stress path coefficient	0.4	default values in the SOSAT
Minimum value of stress path coefficient	0.7	default values in the SOSAT

Introducing these stress state constraints from the Arbuckle formation in Kansas State, the risk of seismicity reduced to 12% as shown in figure 47 below. The uncertainty in the maximum

horizontal stress ranges from 40 – 48 psi shown in figure 46, indicating that the stress state is better constrained. This shows that the geological storage of CO_2 at reduced rates in the Arbuckle formation can be a feasible safe strategy towards achieving climate goals in selected areas and there is value of information in obtaining stress data in these areas.

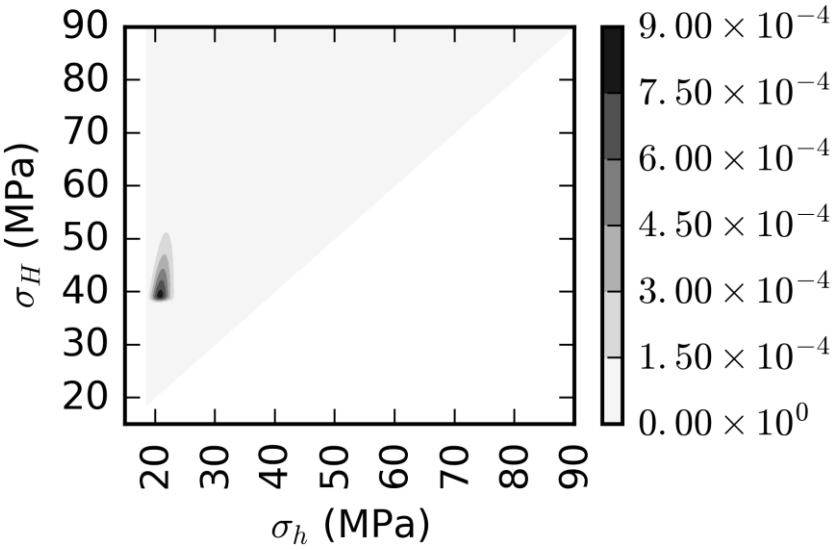

Figure 46:Posterior stress distribution plot

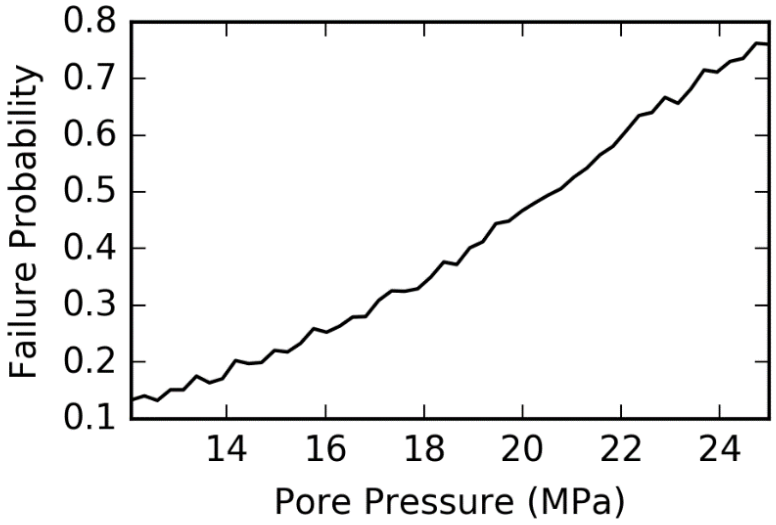

Figure 47: Probability of Fault Activation with Site Specific Stress Data

Future work

Future area of this research entails obtaining site-specific stress data from Oklahoma to reduce uncertainties in maximum horizontal stresses.

CHAPTER 5: Conclusion

The data analysis shows that there is a relationship between the injection of fluid into Arbuckle Group and seismicity, hence, to commence sequestration in the formation, there is need to understand the probability of introducing seismicity in the formation.

The results suggest that we can estimate the probability of inducing seismicity in the formation. Based on our modelling results, at initial injection pressures there is risk of introducing seismicity in the Arbuckle Group, due to the stress state being poorly constrained. Sensitivity analysis determined that the stress regimes, coefficient of friction and stress path had an effect on the shear failure. In most cases analyzed the risk of induced seismicity by injection is still greater than 20% due to the stress state being poorly constrained. Introducing site specific stress from the Arbuckle formation in Kansas State, introduces defined stress state constraints to the model hence reducing risk of seismicity to 12%. Prospect operators and industry stakeholders in the region can enhance their site screening criteria and collect additional data to constrain inherent uncertainties in evaluation of geomechanical risks. Using commonly available data, the Bayesian models which are data-driven can be used for geomechanical risk analysis. This provides value when screening sites and characterizing for GCS, especially when stress data is available. It enables operators to minimize seismicity risks and enables optimized decision-making during operations. The result from this work shows that geological storage of with attention to seismicity risks the Arbuckle Group can be a feasible safe strategy towards achieving climate goals in selected areas and there is value of information in obtaining stress data in these areas.

References

Ajayi, T., Gomes, J., & Bera, A. (2019). A review of CO2 storage in geological formations emphasizing modeling, monitoring and capacity estimation approaches. *Pet. Sci., 16,* 1028-1063. doi:https://doi.org/10.1007/s12182-019-0340-8

Alcalde, J., Flude, S., Wilkinson, M., Johnson, G., Edlmann, K., Bond, C. E., . . . Haszeldine, R. S. (2018). Estimating geological CO2 storage security to deliver on climate mitigation. *Nature Communications, 9,* 2201. doi:https://doi.org/10.1038/s41467-018-04423

Appriou, D. (2019). *Assessment of the Geomechanical Risks Associated with CO2 Injection at the FutureGen 2.0 Site.* PACIFIC NORTHWEST NATIONAL LABORATORY.

Bachu, S. (2008). Storage in Geological Media: Role, Means, Status and Barriers to Deployment. *Process in Energy and Combustion Science,* 254-273.

Bandilla, K. W., Celia, M. A., Birkholzer, J. T., Cihan, A., & Leister, E. C. (2015). Multiphase Modeling of Geologic Carbon Sequestration in Saline Aquifers. *NATIONAL GROUNDWATER ASSOCIATION*. doi:https://doi.org/10.1111/gwat.12315

Barrufet, M. A., Bacquet, A., & Falcone, G. (2010). Analysis of the Storage Capacity for CO2 Sequestration of a Depleted Gas Condensate Reservoir and a Saline Aquifer. *The Journal of Canadian petroleum technology, 49,* 23-31. doi:https://doi.org/10.2118/139771-PA

Battelle, I. (2018, June 5). *Energy & Environment*. Retrieved from Inside Battelle: https://inside.battelle.org/blog-details/carbon-capture-sequestration-is-worth-pursuing?keyword_session_id=vt~adwords|kt~|mt~b|ta~496274902983&_vsrefdom=wor

dstream&gclid=Cj0KCQjwiNSLBhCPARIsAKNS4_dlFUVoYbcC0mSgrfXK4_uxMsRaPRpHD8iUx9DhVJTJe_sVgosxz4gaAqq2E

Benson, S., & Cole, D. (2008). CO2 Sequestration in Deep Sedimentary Formations. *Elements*, 325-331. doi:http://dx.doi.org/10.2113/gselements.4.5.325

Birdie, T., Holubnyak, E., Watney, L., & Hollenbach, J. (2022, 11 25). *Methodology for Constructing Reservoir Maximum Pore Pressure Maps to Meet Class VI Constraints and Prevent Earthquakes.* Retrieved from US Department of Energy: https://www.netl.doe.gov/sites/default/files/netl-file/T-Birdie-Methodology-for-Constructing.pdf

Birdie, T., Holubnyak, E., Watney, L., Bidgoli, T., Hollenbach, J., & Fazelalavi, M. (2022). Assessing Induced Seismicity Risk at the Wellington Geologic Sequestration Site.

Bissell, R. C., Vasco, D. W., Atbi, M., Hamdani, M., Okwelegbe, M., & Goldwater, M. H. (2011). A full field simulation of the In Salah gas production and CO2 storage project using a coupled geo-mechanical and thermal fluid flow simulator. *Energy Procedia, 4*, 3290-3297. doi:https://doi.org/10.1016/j.egypro.2011.02.249

BP Statistical Review of World Energy . (2021). Retrieved from https://www.bp.com/content/dam/bp/business-sites/en/global/corporate/pdfs/energy-economics/statistical-review/bp-stats-review-2021-full-report.pdf

Burghardt, J. (2018). Geomechanical Risk Assessment for. *Rock Mechanics and Rock Engineering*, 1-26. doi:10.1007/s00603-018-1409-1

Burghardt, J. (2021). SOSAT.

Burghardt, J., & Appriou, D. (2021). State of Stress Uncertainty Quantification and Geomechanical Risk Analysis for Subsurface Engineering. *US Rock Mechanics/Geomechanics Symposium.* Houston, Texas, USA: America Rock Mechanics Association.

Chiaramonte, L., Zoback, M. D., Friedmann, J., & Stamp, V. (2008). Seal integrity and feasibility of CO2 sequestration in the Teapot Dome EOR pilot: geomechanical site characterization. *Environmental Geology, 54*(8), 1667-1675. Retrieved from https://idp.springer.com/authorize/casa?redirect_uri=https://link.springer.com/article/10.1007/s00254-007-0948-7&casa_token=RqQmuvF-YcYAAAAA:LSGfogyYy-j6rsjltAO9d13GGnjmOzcBCxluyhH6oO2Esl9731kAQqyHwDUUX82kdeOy6p_Sj9VWwmOzNw

Chidambaram, P., Tewari, R. D., Ali, S. S., Tan, C. P., & PETRONAS, R. S. (2021). Understanding the Effect of Rock Compressibility on CO2 Storage Capacity Estimation in a Depleted Carbonate Gas Reservoir. *International Petroleum Technology Conference.* Virtual: IPTC. Retrieved from https://onepetro.org/IPTCONF/proceedings-pdf/21IPTC/2-21IPTC/D021S003R001/2423471/iptc-21207-ms.pdf

Ching, B. Y., & Friedman, G. M. (2000). Subsurface Arbuckle Group Cambro-Ordovician in the Bowman Well of the Wilburton Field in the Arkoma Basin, Oklahoma; depositional facies, diagenetic signatures, petrophysical aspects, and economic potential. *Carbonates and Evaporites, 15*(1), 49-80. doi:10.1007/bf03175648

Coyle, P. (2018, Nov 1). *What is Bayesian Statistics used for?* Retrieved from Towards Datascience: https://towardsdatascience.com/what-is-bayesian-statistics-used-for-37b91c2c257c

Daneshfar, J., Hughes, R. G., & Civan, F. (2009). Feasibility Investigation and Modeling Analysis of CO2 Sequestration in Arbuckle Formation Utilizing Salt Water Disposal Wells . *Journal of Energy Resources Technology*, 023301-10. doi:10.1115/1.3124115

EPA. (2018). *Geologic Sequenstration of Carbon Dioxide. Underground Injection Control (UIC) Program Class VI Implementaion Manual for UIC Program Directors.*

EPA. (2021). *Subpart UU – Injection of Carbon Dioxide*. Retrieved from United States Environmental Protection Agency: https://www.epa.gov/ghgreporting/subpart-uu-injection-carbon-dioxide#:~:text=This%20rule%20requires%20reporting%20of,purpose%20other%20than%20geologic%20sequestration.

Espinoza, N. D. (2020). *Horizontal Stresses.* Retrieved from Introduction to Energy Geomechanics: https://dnicolasespinoza.github.io/node10.html

Fakher, S., & Imqam, A. (2020). A Review of Carbon Dioxide Adsorption to Unconventional Shale Rocks Methodology, Measurement, and Calculation. *SN Applied Sciences, 2*(1). doi:https://doi.org/10.1007/s42452-019-1810-8

Fakher, S., Abdelaal, H., Elgahawy, Y., & El-Tonbary, A. (2020). A Review of Long-Term Carbon Dioxide Storage in Shale Reservoirs. *Unconventional Resources Technology*

Conferenc. Virtual: Society of Exploration Geophysicists. doi:https://doi.org/10.15530/urtec-2020-1074

Global Change Data Lab. (2022). *Our World in Data*. Retrieved from Annual CO_2 emissions from fossil fuels, by world region: https://ourworldindata.org/grapher/annual-co-emissions-by-region

Gorucu, F. B., Jikich, S. A., Bromhal, G. S., Sams, W. N., Ertekin, T., & Smith, D. H. (2005). Matrix shrinkage and swelling effects on economics of enhanced coalbed methane production and CO 2 sequestration in coal. *Society of Petroleum Engineers Eastern Regional Meeting.* Morgantown, West VA, United States: Society of Petroleum Engineers. Retrieved from https://pennstate.pure.elsevier.com/en/publications/matrix-shrinkage-and-swelling-effects-on-economics-of-enhanced-co

IEAGHG. (2022). *A Brief History of CCS and Current Status*. Retrieved from CCS Information Seet: https://ieaghg.org/docs/General_Docs/Publications/Information_Sheets_for_CCS_2.pdf

Intergovernmental Panel on Climate Change. (2005). *IPSS Special Report onCarbon Dioxide Capture and Storage.* New York: Cambridge University Press. Retrieved from https://www.google.com/url?sa=i&url=https%3A%2F%2Fwww.ipcc.ch%2Fsite%2Fassets%2Fuploads%2F2018%2F03%2Fsrccs_wholereport-1.pdf&psig=AOvVaw1RuofI65_dbVAXQFrgAFD-&ust=1667621358339000&source=images&cd=vfe&ved=0CA0QjhxqFwoTCIiRnOjTk_sCFQAAAAAdAAAAABAR

International Energy Agency. (2016). *20 Years of Carbonn Capture and Storage - Accelerationg Future Deployment.* Cedex, France: OEDC/IEA. Retrieved from chrome-extension://efaidnbmnnnibpcajpcglclefindmkaj/https://iea.blob.core.windows.net/assets/24c3d26b-aa44-4b54-b9c0-5201d4d86a04/20YearsofCarbonCaptureandStorage_WEB.pdf

Jaffar, H., & Abdulnaby, W. (2018). Stress Regime of Rumaila Oilfield in Southern Iraq from Borehole Breakouts. *IOSR Journal of Applied Geology and Geophysics*, 25-35. doi:10.9790/0990-0604022535

Jiang, K., Dou, H., Shen, P., & Sun, T. (2015). China's CCUS Progresses and a New Evaluation Method of CO2 Storage Capacity in Coalbed Reservoirs. *Carbon Management Technology Conference*. Sugar Land, Texas: Society of Petroleum Engineers. doi:https://doi.org/10.7122/440095-MS

Kolawole, F., Johnston, C. S., Morgan, C. B., Chang, J. C., Marfurt, K. J., L. D., . . . M., C. B. (2019). The susceptibiliy of Oklahoma's basement to seismic reactivation. *Nature Geoscience, 12*, 839-844. doi:https://doi.org/10.1038/s41561-019-0440-5

Lakirouhani, A., Detournay, E., & Bunger, A. (2016). A reassessment of in situ stress determination by hydraulic fracturing. *Geophysical Journal International*, *205*(3), 1859-1873. doi: https://doi.org/10.1093/gji/ggw132

McGarr, A., & Barbour, A. J. (2017, September 28). Wastewater Disposal and the Earthquake Sequences During 2016 Near Fairview, Pawnee, and Cushing, Oklahoma. *Geophysical Research Letters, 44*(18). doi:https://doi.org/10.1002/2017GL075258

Murray, K. E. (2013). State-scale perspective on water use and production associated with oil. *Environ. Sci. Technol.,, 47*(9), 4918–4925. doi:https://doi.org/10.1021/es4000593

Nelidov, V. (2021, Novmber 30). *Doing business, the Bayesian way (Part 1)*. Retrieved from Data Driven: https://godatadriven.com/blog/doing-business-the-bayesian-way-part-1/

Oklahoma Corporation Comission. (2021, February 25). *Response to Oklahoma earthquakes*. Retrieved from Oklahoma Corporation Comission: https://oklahoma.gov/occ/divisions/oil-gas/induced-seismicity-and-uic-department/response-oklahoma-earthquakes.html

Oklahoma Geological Survey. (2022, 06 12). *Maps*. Retrieved from Basic Oklahoma Maps: https://www.ou.edu/ogs/maps

Oldenburg, C. M., Bryant, S. L., & Nicot, J.-P. (2009). Certification framework based on effective trapping for geologic carbon sequestration. *International Journal of Greenhouse Gas Control, 3*(4), 444-457. doi:https://doi.org/10.1016/j.ijggc.2009.02.009

Open Data Science. (2021, Aug 5). *6 Applications of Bayesian Methods That You Should Know*. Retrieved from Towards Data Science: https://odsc.medium.com/6-applications-of-bayesian-methods-that-you-should-know-31553f886fe4

Ringrose, P., Mathieson, A., Wright, I., Selama, F., Hansen, O., Bissell, R., . . . Midgley, J. (2013). The In Salah CO2 storage project: lessons learned and knowledge transfer. *Energy Procedia*, 6226-6236.

Rottmann, K. (2018). *Well-Log Characterization of the Arbuckle Group in Central and Northern Oklahoma: Interpretation of the Impact of its Depositional and Post-Depositional History on Injection Induced Seismicity.* Norman: OGS.

Rubinstein, J. L., & Mahani, A. B. (2015). Myths and Facts on Wastewater Injection, Hydraulic Fracturing, Enhanced Oil Recovery, and Induced Seismicity. *Seismological Research Letters, 86*(4), 1060-1067. doi: https://doi.org/10.1785/0220150067

Rutqvist, J. (2012). The Geomechanics of CO2 Storage in Deep Sedimentary Formations. *Geotech Geol Eng, 30*, 525-551. doi:https://doi.org/10.1007/s10706-011-9491-0

Schulz, M., Müller, B., Röckel, T., & Schilling, F. (2020). *Analysis of injection data for pore pressure and minimum horizontal stress magnitude estimates in the Arbuckle Formation.* Karlsruhe Institute of Technology, Institute of Applied Geosciences Division of Technical Petrophysics. doi:DOI: 10.5445/IR/1000105298

Shemeta J. E., Brooks, C. E., & Lord, C. C. (2019). Well Stimulation Seismicity in Oklahoma:. *SEG URTEC Global Meeting*, 95-106. doi:,https://doi.org/10.15530/AP-URTEC-2019-198283

Skoumal, R. J., Ries, R., Brudzinski, M. R., Barbour, A. J., & Currie, B. S. (2018). Earthquakes induced by hydraulic fracturing are pervasive in oklahoma. *Journal of Geophysical Research: Solid Earth*, *123*(12), 10-918.

Snee, J.-E. L., & Zoback, M. (2020). Multiscale variations of the crustal stress field throughout North America. *Nature Communications, 11*, 1951. doi:, https://doi.org/10.1038/s41467-020-15841-5

Stauffer, P. H., Viswanathan, H. S., Pawar, R. J., & Guthrie, G. D. (2009). A system model for geologic sequestration of carbon dioxide. *Environmental Science & Technology, 43*(3), 565-570. doi:https://doi.org/10.1021/es800403w

Verdon, J. P., Kendall, J. M., White, D. J., & Angus, D. A. (2011). Linking microseismic event observations with geomechanical models to minimise the risks of storing CO2 in geological formations. *Earth and Planetary Science Letters, 305*(1-2), 143-152. doi:https://doi.org/10.1016/j.epsl.2011.02.048

Walsh, F. R., & Zoback, M. D. (2015). Oklahoma's recent earthquakes and saltwater disposal. *Science advances, 1*(5).

Weingarten, M., Ge, S., Godt, J. W., Bekins, B. A., & Rubinstein, J. L. (2015). High-rate injection is associated with the increase in us mid-continent seismicity. *Science, 348*(6241), 1336-1340.

White, J. A., Foxall, W., C. Bachmann, L. C., & Daley, T. (2015). *Induced seismicity and carbon storage: Risk assessment and mitigation strategies.* Lawrence Livermore National Security, LLC.

Wikipedia. (2022, Feb 23). *Bayesian network*. Retrieved from https://simple.wikipedia.org/wiki/Bayesian_network

Wikipedia. (2022, October 19). *Cluster analysis*. Retrieved from Wikipedia: https://en.wikipedia.org/wiki/Cluster_analysis

Zhou, Q., Birkholzer, J. T., Mehnert, E., Lin, Y. F., & Zhang, K. (2010). Modeling basin-and plume-scale processes of CO2 storage for full-scale deployment. *Groundwater, 48*(4), 494-514. doi:https://doi.org/10.1111/j.1745-6584.2009.00657.x

Zoback, M. D., Barton, C. A., Brudy, M., Castillo, D. A., Finkbeiner, T., Grollimund, B. R., . . . Wiprut, D. J. (2003). Determination of stress orientation and magnitude in deep wells. *International Journal of Rock Mechanics and Mining Sciences, 40*(7-8), 1049-1076. Retrieved from https://www.sciencedirect.com/science/article/pii/S1365160903001175?casa_token=RYGyEByIyeQAAAAA:tEGwyhOEPIpfGp78Y-skeK_HH0Piy0wDSRIVzJJ2Flh0LQgXAbyG9a0rKw1Td30KaORdxJi_RVM

NOMENCLEATURE

σh	principal minimum horizontal stress
σH	principal maximum horizontal stress
σv	principal vertical stress
μ	friction coefficient
Γh	stress path coefficient
CO_2	Carbon dioxide
COP26	United Nations Climate Change Conference
CUSP	Carbon, Utilization, Storage Partnership
EOR	Enhanced Oil Recovery
GCS	Geological Carbon Storage
MPa	Megapascals
Psi	Pound square inch
Shmin	principal minimum horizontal stress
SHmax	principal maximum horizontal stress
SOSAT	State of Stress Analysis Tool
Sv	principal vertical stress

APPENDIX

SOSAT

Hardware requirements

- 64-bits Windows Operating System
- Space is not a major constraint

Software requirements

- Java Runtime Environment (JRE) – 8 or a later version
- Steps to download included below

Installation

- SOSAT version 1.0 is available at the National Energy Technology Laboratory (NETL) Energy Data Exchange (EDX) platform for download
- First step is to sign into EDX https://edx.netl.doe.gov/
- You might need access from NETL to be able to sign in
- After signing in, navigate to the zipped folder SOSAT folder at https://edx.netl.doe.gov/dataset/sosat-state-of-stress-analysis-tool-v2019-07-1-0
- Then download the zipped folder named nrap-sosat-v2019.07-1.0.zip to the hard drive of your
- Extract the files from the folder in preparation for installation

- Download Java Runtime Environment (JRE) 8 or a later version. If you have JRE already on your computer skip the next couple of steps.
- Navigate to https://www.oracle.com/java/technologies/downloads/
- Scroll down to Java SE Development Kit
- Select the operating system, SOSAT has been designed to run on Windows
- SOSAT requires a 64-bit environment so select the x64 Installer
- If you had java before, ensure your JAVA-HOME is set to the version 8 runtime environment
- To do this, in your PC search bar, search for environment variables

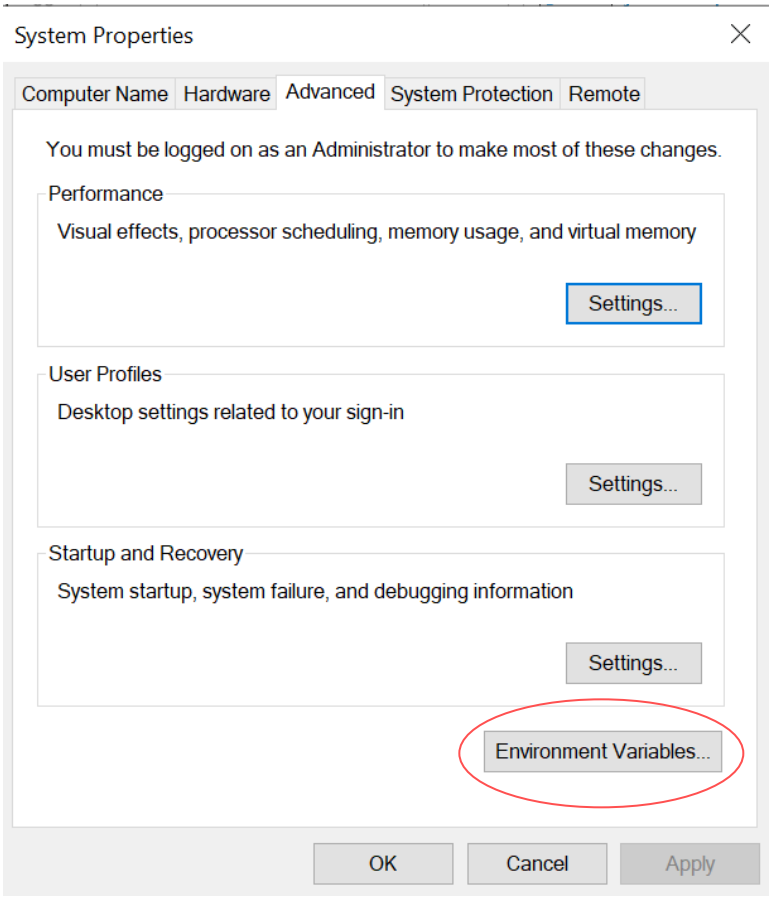

Figure 48: Environment Variables

- Select Environment Variables as highlighted above
- Ensure the JAVA_HOME and JRE_HOME are set to the java 8 runtime environment as shown below.

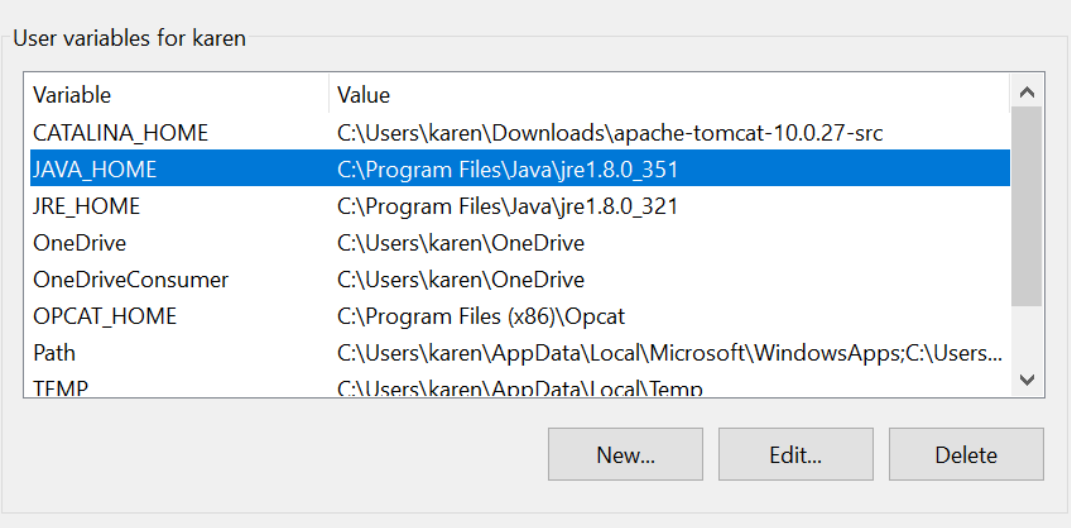

Figure 49: Updating JAVA_HOME and JRE_HOME

- After downloading and installing Java, go back to your SOSAT downloaded folder
- Click on the application.bat file in the folder and run
- If the JAVA_HOME and JRE_HOME are not set to the right version, SOSAT would run into an error and the main page would not appear. Circle back to previous steps and ensure these are set up well
- After installation, you would receive a Notice to User, acknowledge this and you would be redirected to the SOSAT Main Page shown below

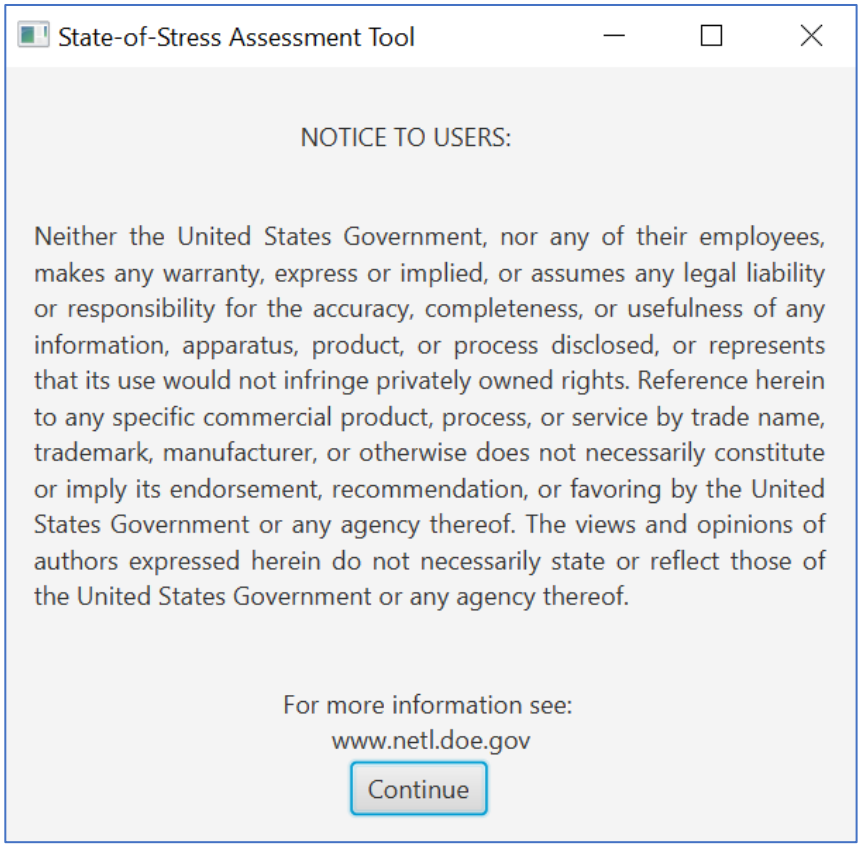

Figure 50: Notice to Users

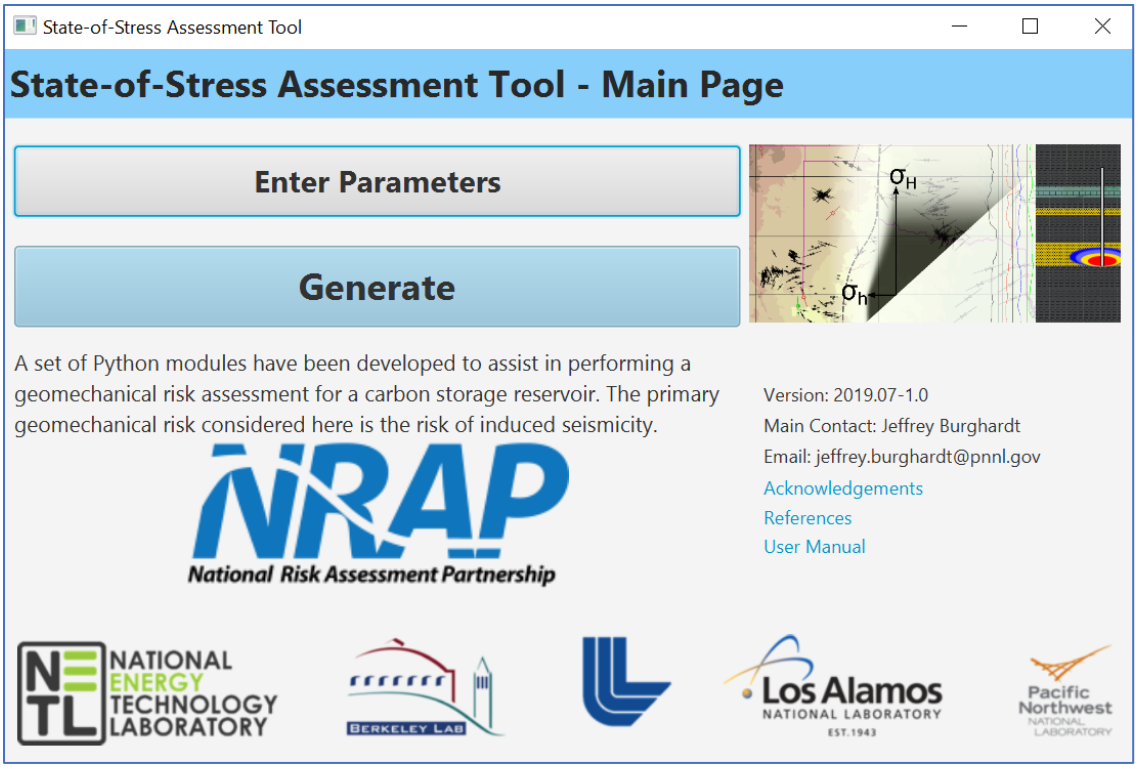

Figure 51: SOSAT Main Page

- The next step is to click on enter parameters in the tab shown below to enter the required parameters as defined in chapter 2 of this report

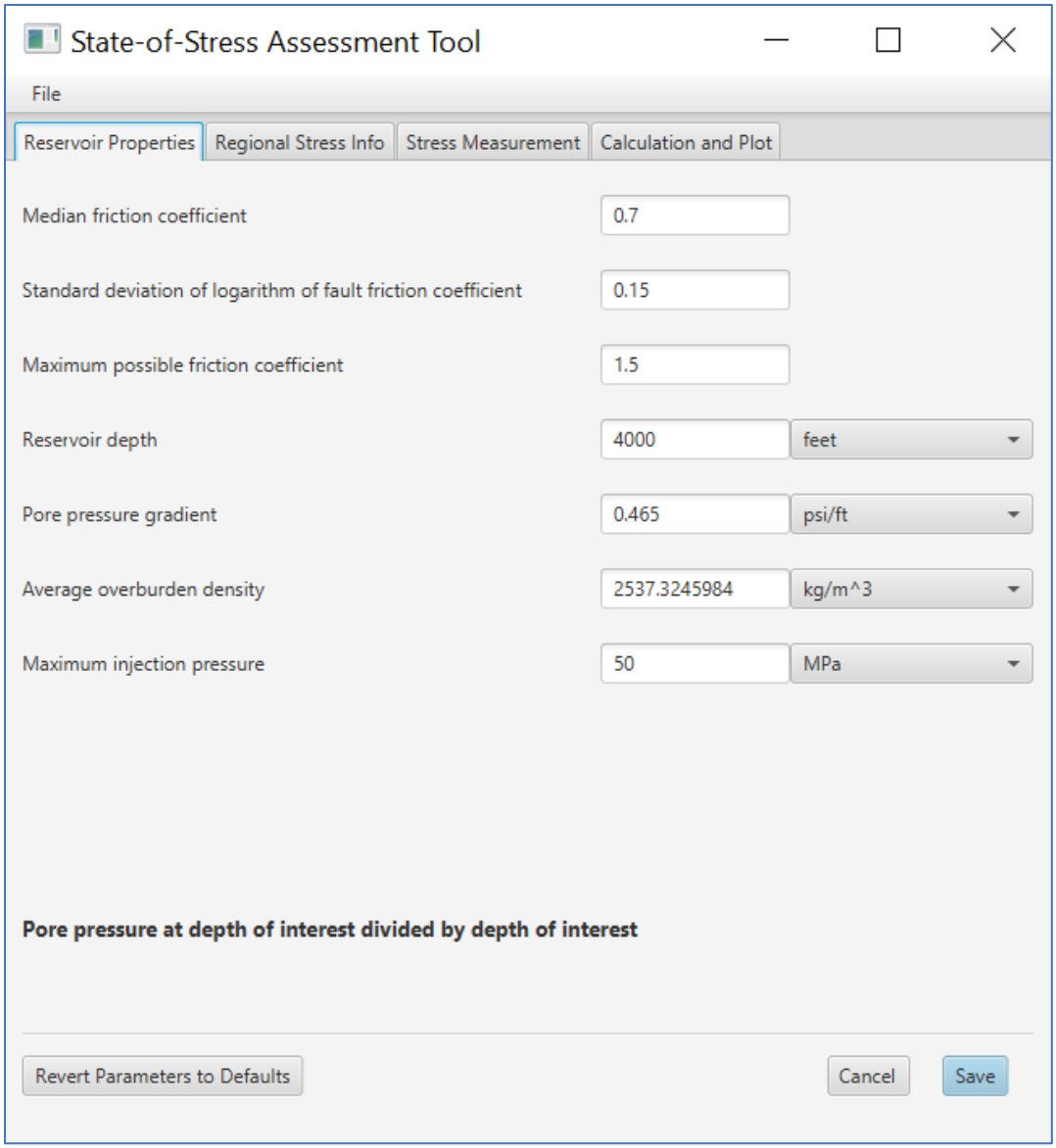

Figure 52: Enter Parameters in SOSAT

- Enter the reservoir properties, regional stress information, stress measurement information and the calculate and plot
- In the calculation and plot tab, don't forget to specify the directory where the plots would be stored as shown below.

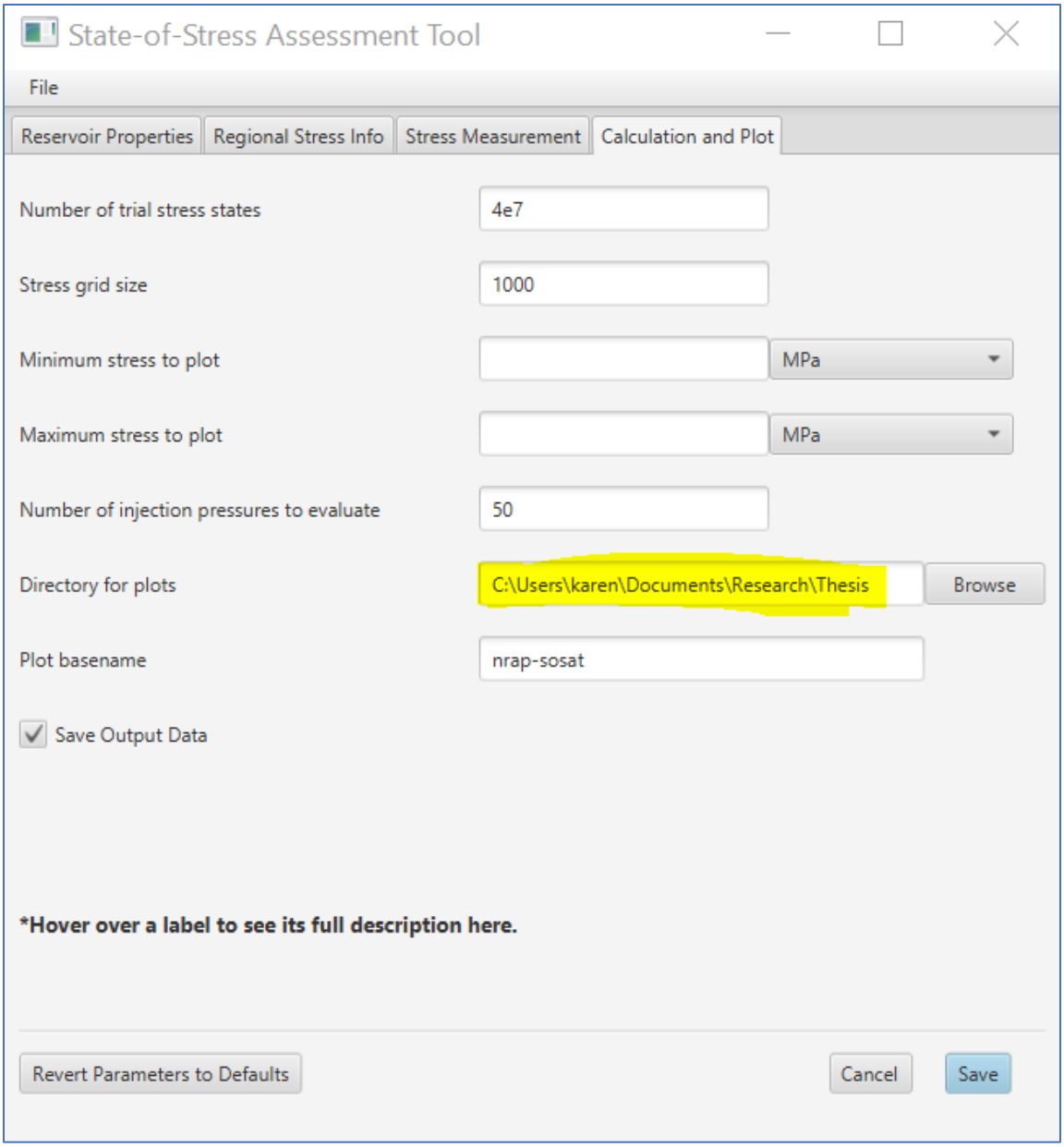

Figure 53: Including file directory

- After clicking save, you would be directed to the Min Page where you click generate and this would launch the analysis routine as shown below

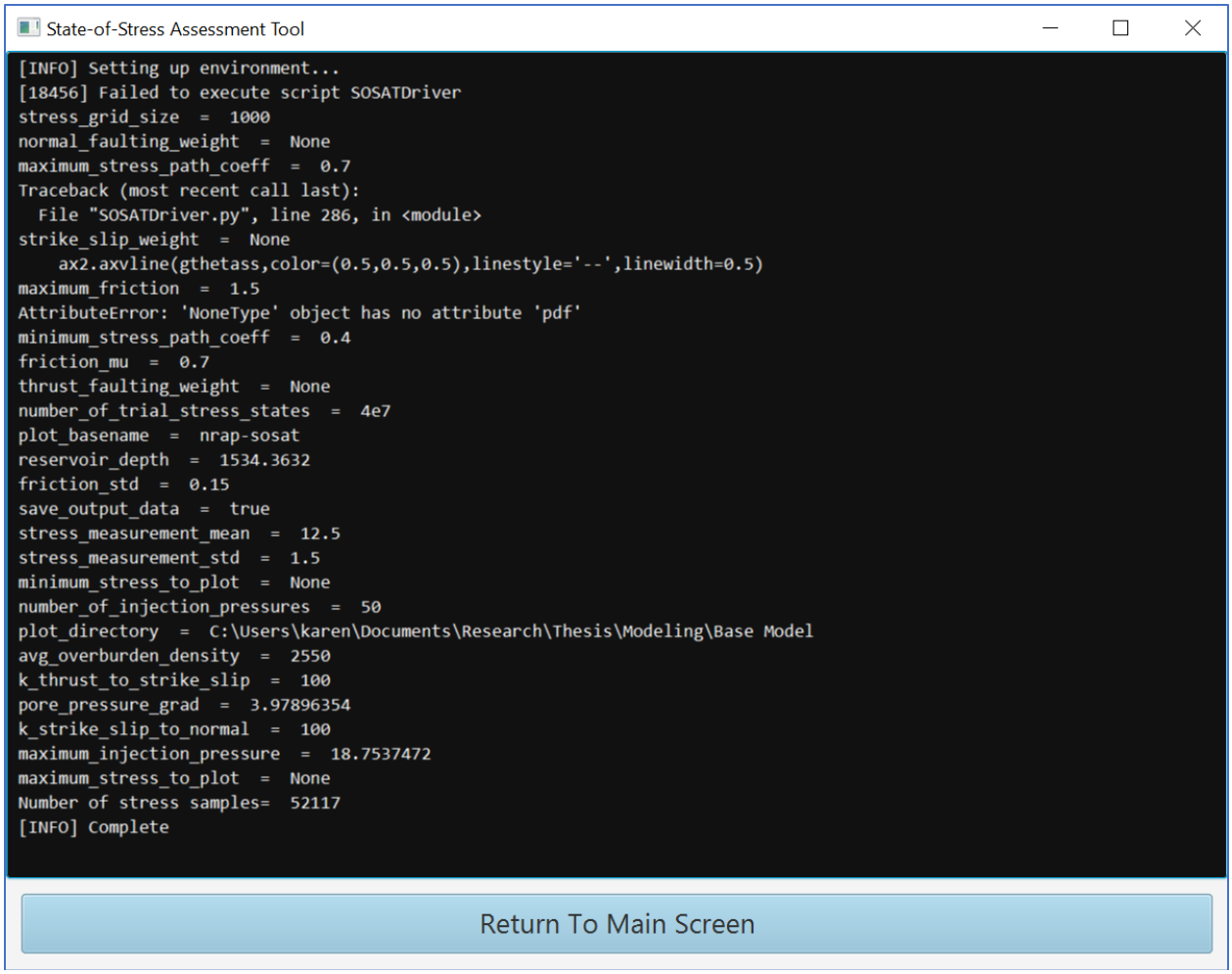

Figure 54: Running analysis